Geological Magazine

www.cambridge.org/geo

Original Article

Cite this article: Chandra R, Kowser N, Brookfield ME, Satyanarayanan M, and Stöckli D (2023) Nature of the Shyok (Northern) Suture Zone between India and Asia: petrology, geochemistry and origin of the Tirit granitoids and associated dykes (Nubra Valley Ladakh Himalaya, NW India). *Geological Magazine* **160**: 1020–1039. https://doi.org/10.1017/S0016756823000134

Received: 1 July 2022
Revised: 17 February 2023
Accepted: 17 February 2023
First published online: 3 April 2023

Keywords:
Granitoids; dykes; enclaves; magmatism; geochronology; subduction

Author for correspondence: ME Brookfield, Email: mbrookfi@gmail.com

Nature of the Shyok (Northern) Suture Zone between India and Asia: petrology, geochemistry and origin of the Tirit granitoids and associated dykes (Nubra Valley Ladakh Himalaya, NW India)

Rakesh Chandra[1], Nazia Kowser[1], Michael E Brookfield[2], Manavalan Satyanarayanan[3] and Daniel Stöckli[2]

[1]Department of Earth Sciences, University of Kashmir, Srinagar 190 006, India; [2]Jackson School of Geosciences, University of Texas at Austin, Austin, TX 78712, USA and [3]CSIR – National Geophysical Research Institute, Hyderabad 500 007, India

Abstract

The Shyok Suture Zone is an oceanic remnant of the Neo-Tethyan ocean sandwiched between the Ladakh Batholiths to the south and Karakoram Batholith to the north. The Tirit granitoids in this suture are dark-coloured, relatively rich in ferromagnesian minerals and range from granodiorite–tonalite to gabbro–diorite in composition. Mafic igneous enclaves are quite common and they are intruded by NW–SE parallel doleritic and aplitic dykes. The Tirit granitoids have a wide range of major oxide compositions (SiO_2 = 52.1–72.11 wt %, TiO_2 = 0.21–1.23 wt %, Al_2O_3 = 11.42–13.52 wt %, MgO = 1.69–10.69 wt % and CaO = 3.24–9.31 wt %) and show calc-alkaline, metaluminous, I-type characteristics, transitional between primitive and mature arc continental plutons. Rare earth elements (REE) show considerable enrichment in light REE (LREE) as compared to the heavy REE (HREE). Late Cretaceous U/Pb dates (74–68 Ma) show that they formed during the pre-collision northward movement of India. The Tirit dykes are only slightly younger and probably part of the same episode.

1. Introduction

The age and nature of the crust and the timing of ocean basin closure are keys to understanding the evolution of suture zones (Dewey, 2005; Stern *et al.* 2012; Draut & Clift, 2013). Critical to developing accurate tectonic reconstructions of such sutures are detailed mapping and analysis of their usually complex and highly deformed rock suites (Dewey, 1977; Frassi *et al.* 2016; Saktura *et al.* 2021*b*).

The Shyok (Northern) Suture Zone (SSZ) is the northernmost of two sutures that can be traced across the NW Himalayan syntaxis, from the Chaman fault zone to the Karakoram fault zone (Fig. 1), both of which are complex mid- to late Cenozoic collisional transform faults which connect the N-directed thrust of the North Pamir to the S-directed thrusts of the Makran and Southern Tibet (Zhang *et al.* 2011; Brookfield *et al.* 2017; Wallis & Searle, 2019). East of the Karakoram fault zone, the southern Indus Suture Zone (ISZ) is usually equated with the Yarlung–Tsangpo suture zone (Hébert *et al.* 2012), while the SSZ is usually equated with the Bangong suture separating southern and central Tibet (Rolland *et al.* 2009; Parsons *et al.* 2020). The SSZ, however, may be equivalent to the Luobadui–Milashan Fault with eclogites and blueschists in eastern Tibet, which separates the southern Lhasa block, with the Gangdise Batholiths, from the central Lhasa block, with a complete Palaeozoic section comparable with that of the Karakoram block (Gaetani, 1997; Zhu *et al.* 2013; Liu *et al.* 2017; Yogibekov *et al.* 2020). The early Cretaceous Bangong suture zone is more likely equivalent to the Rushan–Pshart suture between the Central and South Pamir blocks (Schwab *et al.* 2004). West of the Chaman Fault Zone, the SSZ may be equivalent to the less compressed Kandahar fore-arc and Ras Koh arc (Kassi *et al.* 2007; Shroder *et al.* 2021) (Fig. 1). The nature and equivalence of the SSZ is nevertheless debatable. The SSZ is at altitudes of over 3000 m within even higher mountainous terrain, and is difficult to access in places, not only because roads and tracks are limited, but because it lies in politically disputed zones between Pakistan, India and China (Fig. 2a). Studies have been made in the areas on either side of the India–Pakistan line of control (summarized in Pudsey, 1986; Robertson & Collins, 2002; Rolland *et al.* 2009; Borneman *et al.* 2015), but the age and nature of components of the SSZ are still unresolved, as illustrated by the very different and incompatible geological maps published of the area (e.g. Rai, 1982; Dunlap & Wysoczanski, 2002; Saktura *et al.* 2021*b*). Estimates of the age of formation of the SSZ range

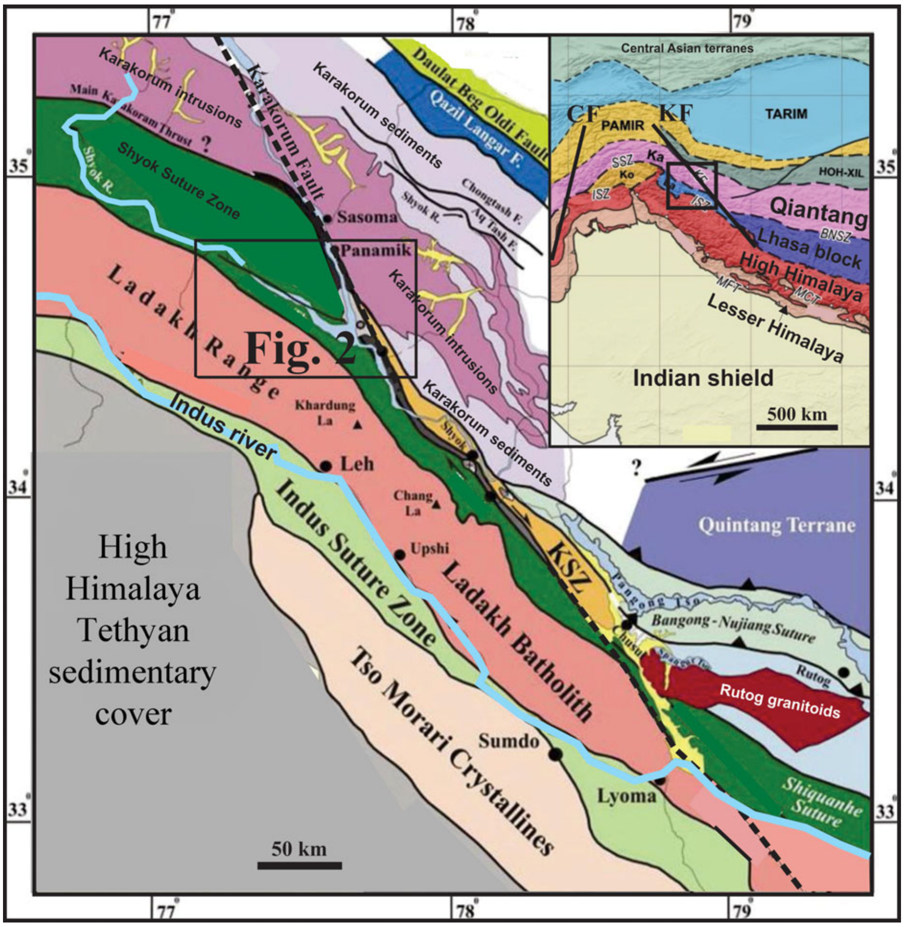

Fig. 1. (Colour online) Geological map of Ladakh, showing location of Figure 2 (from Jain, 2014). Inset shows location of map on terrane map of India–Asia collision zone (from Parsons *et al.* 2020). CF – Chaman fault; KF – Karakoram fault; Ko – Kohistan arc; Ka – Karakoram.

from Cretaceous (Weinberg *et al.* 2000; Rolland *et al.* 2006; Rehman *et al.* 2011) to Eocene (Khan *et al.* 2009).

Detailed study of the individual components of the SSZ is needed in order to resolve its nature, development and age. We here discuss the petrology, geochemistry, age and nature of the Tirit granitoids and associated dykes at the Nubra–Shyok confluence, using a map based on Borneman *et al.* (2015) and our own extensive fieldwork in the area (Fig. 2).

2. Geological overview

In the Nubra–Shyok confluence area, the SSZ forms a narrow highly tectonized belt, overthrust in the south by the Ladakh batholith and in the north by the Karakoram batholith (Fig. 2b, c; Rai, 1983; Upadhyay *et al.* 1999; Rolland *et al.* 2000; Borneman *et al.* 2015). The dominant rocks are ophiolitic fragments, basic to acid volcanics and intrusives, pelagic oceanic sediments, cherts and foraminiferal limestones similar to those of the ISZ to the south, with large olistoliths of Asian shelf sediments in places (Brookfield & Gupta, 1984; Rolland *et al.* 2000; Robertson & Collins, 2002; Upadhyay, 2014; Upadhyay *et al.* 2014). All these have been highly tectonized and are unconformably overlain in Ladakh by coarse continental clastics of post-Oligocene age (Rai, 1982).

The SSZ has various and divergent interpretations as: an oceanic suture (Gansser, 1977); a subduction zone, older than (Petterson & Windley, 1985) or younger than (Brookfield & Reynolds, 1981; Reynolds *et al.* 1983) the ISZ; a tectonic repetition of the ISZ (Rai, 1982, 1983; Srimal, 1986); a back-arc complex related to the ISZ (Thakur & Misra, 1984; Dunlap & Wysoczanski, 2002); and a marginal basin (Upadhyay, 2002). A popular view is that the SSZ is a site of probably Early to Late Cretaceous Ocean closure, while the ISZ is the younger main suture between the Indian continental plate and Asian continental plate (Srimal, 1986; Upadhyay *et al.* 1999; Rolland *et al.* 2000; Robertson & Collins, 2002; Bhutani *et al.* 2009; Upadhyay, 2009; Borneman *et al.* 2015; Kumar *et al.* 2016).).

South of the SSZ, the Ladakh block is mostly calc-alkaline batholiths and their extrusive equivalents (the Khardung Volcanics), with pendants and enclaves of pre-intrusive country rocks that include the Changmar and Shoyk Volcanics described below (Weinberg *et al.* 2000; Rolland *et al.* 2002*b*; Thanh *et al.* 2010; Saktura *et al.* 2021*a*). The Ladakh batholiths consist mostly of coarse- to fine-grained granite to diorite intrusions with roof pendants and enclaves of ophiolites (Reuber, 1990; Rolland *et al.* 2000), coarse mafic and acid intrusives (Kumar, 2010) and sedimentary rocks (Raz & Honegger, 1989). U/Pb zircon dates indicate that magmatism was concentrated during a 20 million year period from ~65 Ma to ~45 Ma (St-Onge *et al.* 2010; White *et al.* 2011). More basic intrusives on the north range give U/Pb of ~66 to 60 Ma, whereas the main granite intrusions give a U/Pb date of ~50 Ma (St-Onge *et al.* 2010; Thanh *et al.* 2010; Shellnutt *et al.* 2014). These correspond to two main episodes of magmatism, with a change in composition from I-type to S-type granites and adakites, attributed to crustal thickening during the 'hard' collision between Indian and Asian continental crust (Shellnutt *et al.* 2014).

https://doi.org/10.1017/S0016756823000134 Published online by Cambridge University Press

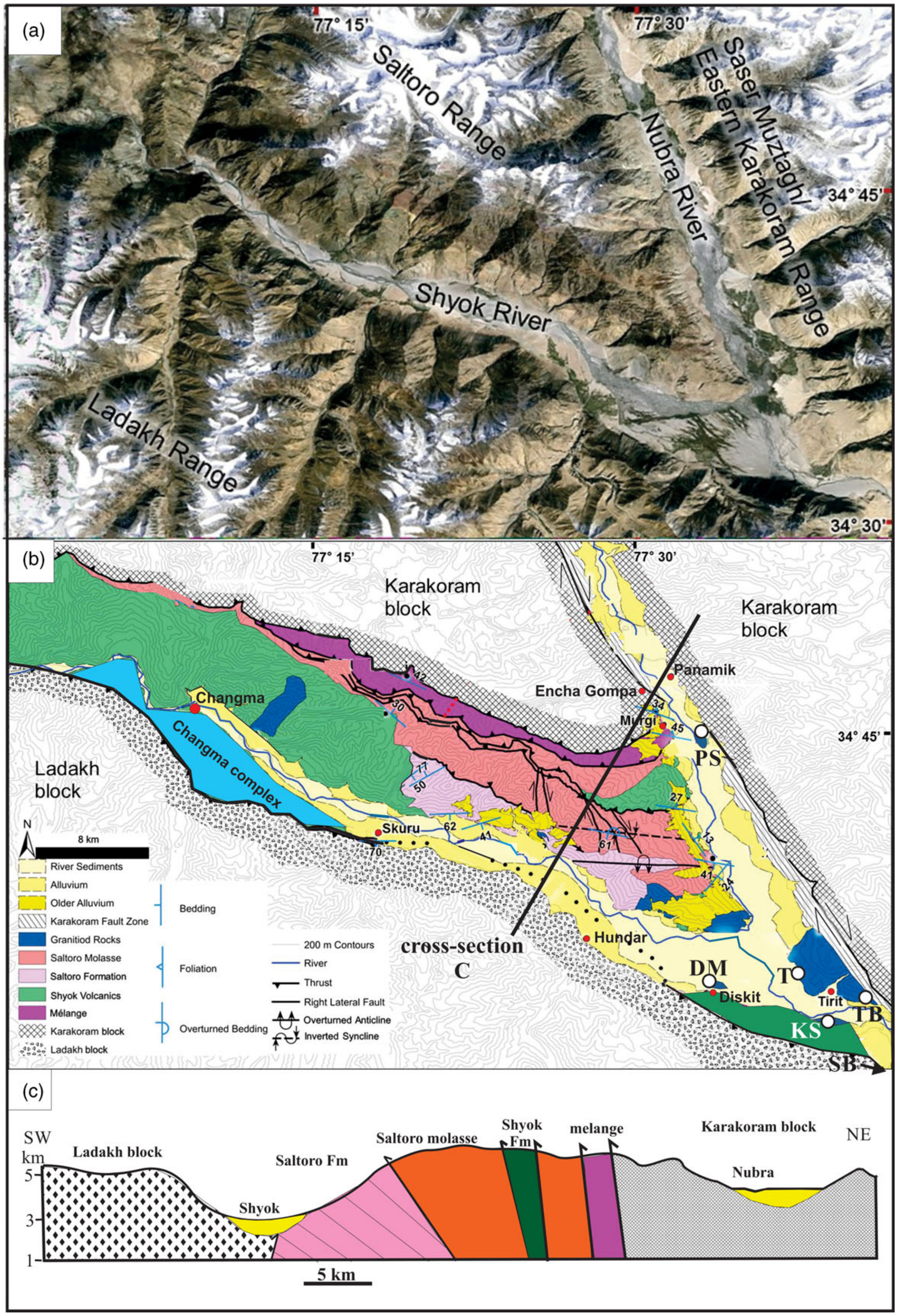

Fig. 2. (Colour online) (a) Satellite view of study area. (b) Geological map of study area, modified from Borneman *et al*. (2015), with changes from Saktura *et al*. (2021*b*) and authors' field observations, showing location of samples; cross-section modified from Upadhyay *et al*. (1999) and Borneman *et al*. (2015).

https://doi.org/10.1017/S0016756823000134 Published online by Cambridge University Press

On the northern side of the Ladakh Range, the Khardung Volcanics overlie, are intruded by and are overthrust by the Ladakh batholith (Upadhyay *et al.* 1999; Rolland *et al.* 2000; Weinberg *et al.* 2000). The Khardung Volcanics consist of basalts, andesites, dacites, rhyodacites and rhyolites with associated pyroclastics, and become more acidic upwards (Upahdyay, 2014). The lower andesites (U/Pb zircon date of ~70 Ma) switch to rhyolites (U/Pb zircon dates of ~65 ± 2 Ma), and these persist until ~52 Ma (Lakhan *et al.* 2020; Saktura *et al.* 2021*a*), with Ar/Ar whole-rock dates of ~55 Ma (Bhutani *et al.* 2009; White *et al.* 2011). Like the Ladakh batholith, the volcanics become more acidic upwards and are thus likely co-magmatic with it, as they have comparable ages.

From south to north, the units in the Shyok belt are as follows:

1. The Changmar complex consists of norites, gabbronorites, plagiogranites, harzburgites and serpentinites (Saktura *et al.* 2021*b*). It is intruded by the Ladakh Batholith, intrudes the Shyok Volcanics to the north and possibly forms the oceanic substrate to the Shyok volcanic arc (Rolland *et al.* 2000; Saktura *et al.* 2021*b*).
2. The Shyok Volcanics consist of calc-alkaline basaltic to andesitic volcanics metamorphosed to greenschist facies (Weinberg *et al.* 2000; Thanh *et al.* 2012; Sivaprabha *et al.* 2022). Along the Shyok River, the unit is intruded by gabbroic dykes probably related to the Changmar conplex (Saktura *et al.* 2021*b*). One of the dykes gave a Lower Cretaceous $^{40}Ar/^{39}Ar$ hornblende age of 125.6 ± 6.1 Ma (Aptian) (Borneman *et al.* 2015).
3. The Saltoro Formation is overthrust by the Kharduing Volcanics south of Khalsar, but may rest unconformably on the Shyok Volcanics to the northwest (Upadhyay *et al.* 1999; Borneman *et al.* 2015) (Fig. 2). The lower part, sometimes separated out as the Tsoltak Formation, consists of deeper water thinly and mostly even-bedded, highly fissile and cleaved slates, phyllites, and siltstones, with intercalations of thinly to medium-bedded grey fossiliferous limestones and marbles, with possibly late Jurassic bryozoa (Upadhyay *et al.* 1999). A tectonically isolated thick recrystallized limestone, called the Hundiri Formation, contains abundant mollusc and Lower Cretaceous (Aptian – early Albian) foraminifera (Juyal, 2006). To the southeast, the lower part of the formation contains Middle Jurassic (Callovian) ammonites (Ehiro *et al.* 2007). The upper part of the Shyok Formation consists of shallower-water sandstones and mudstones with bivalves and gastropods passing up into Lower Cretaceous (Albian) limestone conglomerates and acidic tuffs (Matsumaru *et al.* 2006). The age of the Saltoro Formation overlaps with that of the Shyok Volcanics and may be a back-arc basin to a Shyok Volcanic oceanic arc (Upadhyay *et al.* 1999).
4. The Saltoro Molasse consists of coarse- to fine-grained continental clastic sediments, at least 3.2 km thick, unconformable on, and overthrust onto, the Shyok Volcanics and Saltoro Formation (Rai, 1983). The rounded fluvial orthoconglomerate pebbles range from 0.1 to 1 m, and are dominated by Shyok Volcanic greenstones, with subordinate granite, phyllites and schists (Rai, 1983). The molasse is a typical deposit of near-source alluvial fans (Blair & McPherson, 2009).
5. An ophiolitic mélange is the topmost unit within the Shyok suture zone, overthrusts the Saltoro Molasse and is overthrust by the Karakoram block (Weinberg *et al.* 2000). It is *c.* 1 km thick and contains decimetre- to kilometre-scale blocks of phyllite, limestone, red chert, basalt, gabbro and peridotite (Rai, 1983).

Numerous felsic to mafic dykes also cut all SSZ units, except the ophiolitic mélange, and thus predate the southward thrusting of the Karakoram block. Some individual dykes can be traced over 1 km in the field. The felsic to intermediate composition dykes typically have an aplitic texture and are often heavily altered and crumbly in hand specimen.

6. The Karakoram block overthrusts the ophiolitic mélange, and consists of metamorphosed Palaeozoic to Upper Cretaceous host rocks (Rai, 1983; Sinha *et al.* 1999; Rolland *et al.* 2002*a*) intruded by Lower Cretaceous (110–100 Ma) calc-alkaline and Upper Cretaceous (85 Ma) alkaline granitoids. This Cretaceous magmatism is attributed to the development of an Andean arc on the southern edge of Asia (Rolland *et al.* 2002*b*). Younger Cenozoic collisional magmatism and metamorphism occurred in several phases during the hard collision of India and Asia (Rolland *et al.* 2001), with Oligocene to Miocene (26 to 21 Ma) leucogranites intruded during thrusting of the Karakoram block over the SSZ and right-lateral displacement on the Karakoram Fault (Schärer *et al.* 1990; Allen & Chamberlain, 1991; Debon & Khan, 1996; Rolland *et al.* 2001, 2006, 2009; Horton & Leech, 2013; Brookfield *et al.* 2017; Pundir *et al.* 2020).

3. Tirit granitoids and associated dykes

Tirit granitoid and dyke samples were collected at outcrops at Khalsar (KS), Tegart (T), Diskit (DM), Tirit Bridge (TB) and Sati Bridge (SB) (Fig. 2).

3.a. Tirit granitoids

The Tirit granitoids outcrop in four areas: around Tirit, north and south of Diskit and northeast of Hundar. They intrude the Saltoro Formation, and are faulted against the Karakoram block at the Karakoram Fault Zone east of Tirit (Figs 3 and 4a). These outcrops were originally a single plutonic body and are now isolated by a cover of Quaternary alluvium (Rao & Rai, 2009). The granitoids are dark-coloured, relatively rich in ferromagnesian minerals and range from granodiorite–tonalite to gabbro–diorite in composition. Mafic sub-rounded to rounded igneous enclaves up to 30 cm in diameter are quite common in these granitoids and possibly derive from the Shyok Volcanics (Fig. 4).

3.b. Dykes

Mafic dykes intrude the Tirit granitoids east of Tirit at Sati Bridge (SB) (Fig. 2), The NE–SW-trending parallel mafic dykes are doleritic (Fig. 4e), with thicknesses varying between 30 cm and 1.5 m, and displaced up to 0.5 m by post-emplacement faulting (Fig. 4f). They show no evidence of chilling against the walls of granitoids, indicating that the host rocks were still hot when the dykes intruded. They are comparable in orientation and possibly age, but not in composition, to E–W- and NE–SW-striking late-stage andesitic dykes of the Ladakh batholith (~45 Ma) west of Leh (Heri *et al.* 2015).

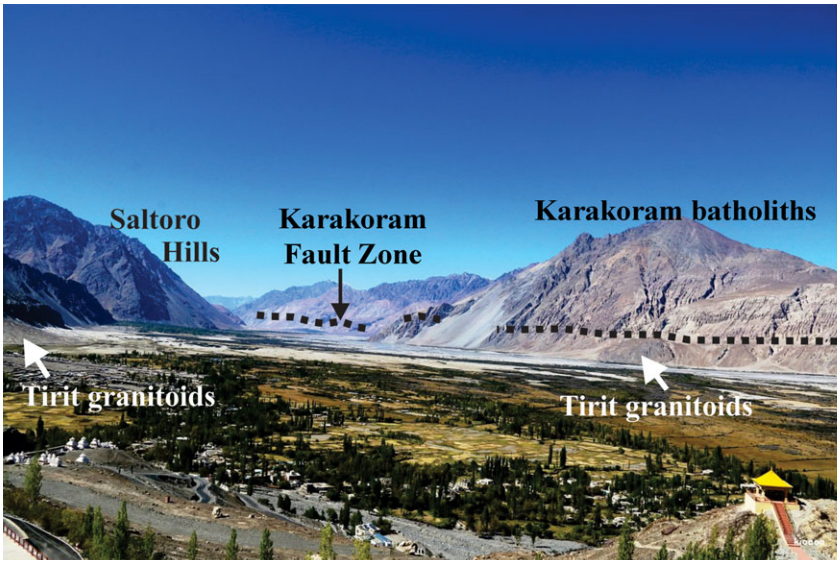

Fig. 3. (Colour online) View up Nubra valley from Diskit showing eastern outcrops of Tirit granitoids.

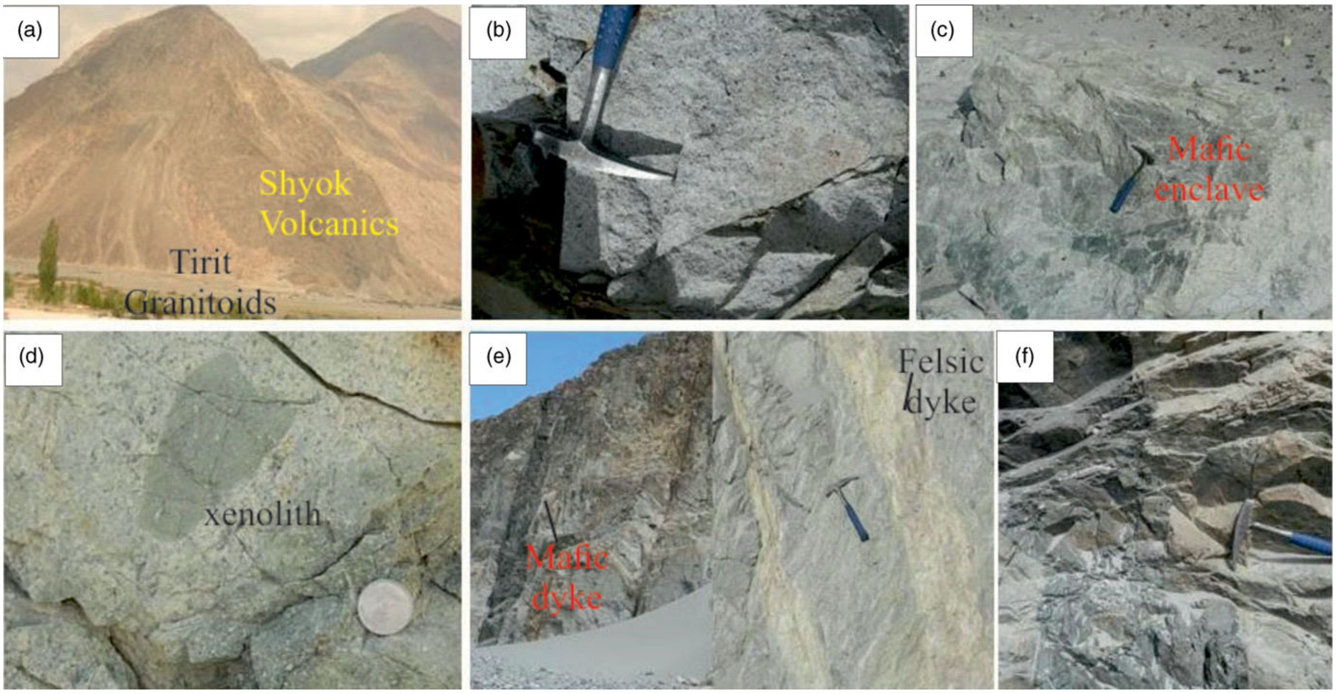

Fig. 4. (Colour online) Field photographs showing (a) intrusive contact of Tirit granitoids with Shyok Volcanics near Tirit Village Nubra Valley; (b) Tirit granitoids relatively rich in ferromagnesian minerals; (c) diffuse mafic enclaves in Tirit granitoids at Tirit Bridge, Nubra Valley; (d) xenoliths in Tirit granitoids at Tegar, Nubra Valley; (e) mafic and felsic dykes in Tirit granitoids near Tirit Bridge; (f) displacement of mafic enclave in Tirit granitoids near Tirit Bridge.

3.c. Petrography

3.c.1. Tirit granitoids

Major minerals are plagioclase, K-feldspar, quartz, biotite and hornblende, with zircon and magnetite as accessory minerals (Fig. 5). Point counts show that: the granites have 24–27 % K-feldspar, 5–7 % plagioclase and 14–22 % quartz; the granodiorites have 9–34 % K-feldspar, 11–19 % plagioclase and 15–29 % quartz; the trondhjomites have 20–29 % K-feldspar, 29–35 % plagioclase and 2–16 % quartz; and the quartz–diorites have 14–23 % K feldspar, 14–16 % plagioclase, and 20–24 % quartz. Euhedral plagioclase laths within subhedral grains of K-feldspar and quartz signify early increments of growth (Fig. 5a), followed by later development of K-feldspar and quartz grains which show graphic intergrowths (Fig. 5b). Quartz grains have undulose extinction and cataclastic textures in places (Fig. 5c). Some biotite grains show chloritization (Fig. 5d), and some plagioclase grains show sericitization (Fig. 5e); while both show marginal epidotization in places (Fig. 5f), indicating hydrothermal alteration.

3.c.2. Dykes

The mafic dykes are dark grey to black, and fine- to medium-grained in texture. Major minerals are plagioclase, clinopyroxene and magnetite, with accessory amounts of chlorite and opaque mineral phases. They commonly exhibit porphyritic texture with

https://doi.org/10.1017/S0016756823000134 Published online by Cambridge University Press

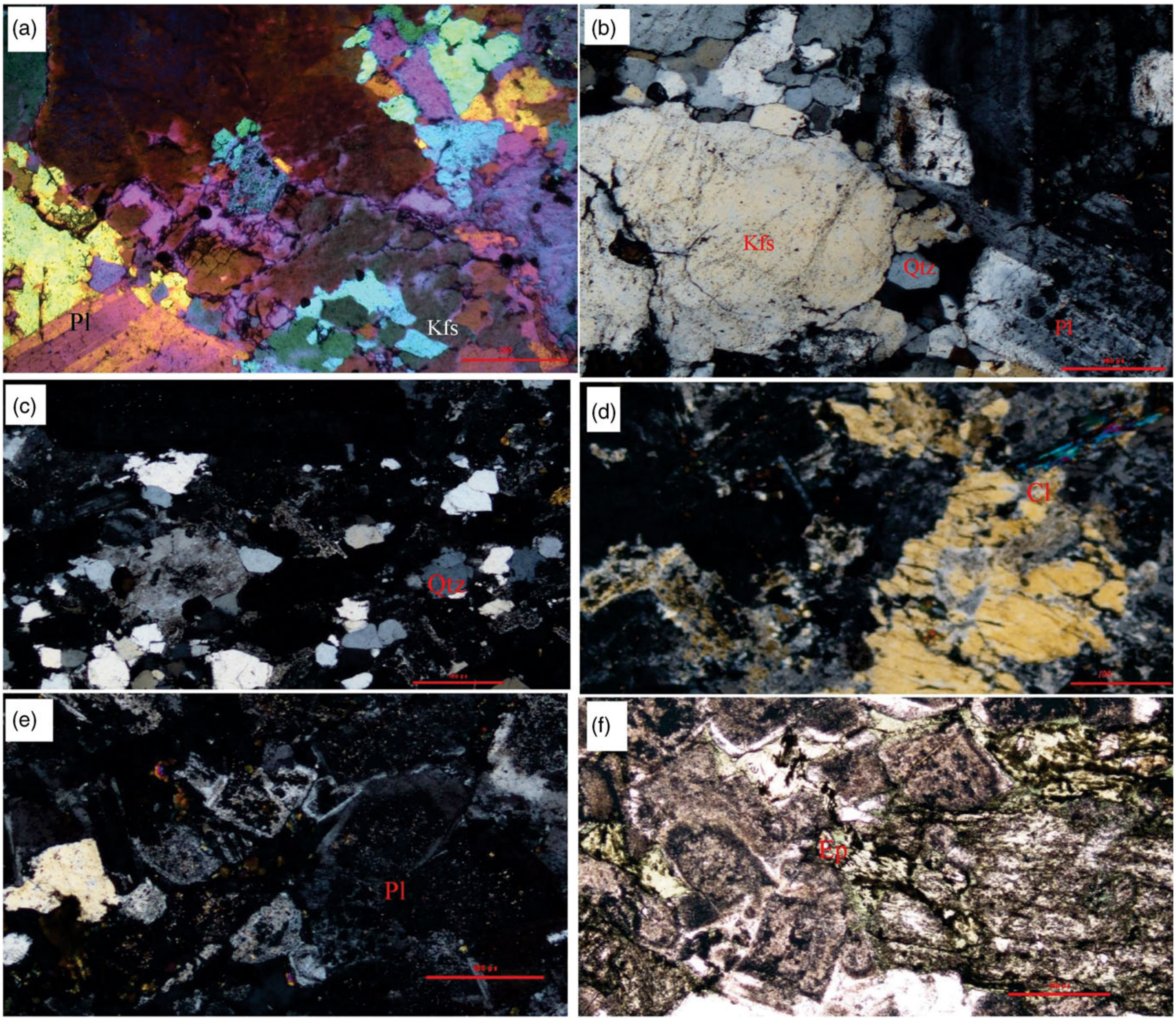

Fig. 5. (Colour online) Photomicrographs of Tirit granitoids showing (a) plagioclase laths enclosed within subhedral grains of K-feldspar and quartz (PPL); (b) plagioclase with euhedral crystal faces in contact with K-feldspar and quartz grains (XPL); (c) plagioclase mineral grains exhibiting simple and polysynthetic twinning; (d) epidotization at the margins of plagioclase and biotite mineral grains (XPL); (e) alteration of biotite into green chlorite and the sericitization of plagioclase (XPL); and (f) epidotization of biotite, alteration of plagioclase and zircon inclusions (XPL). Kfs: K-feldspar; Qtz: quartz; Bt: biotite; Zr: zircon; Pl: plagioclase; Cl: chlorite; Ms: muscovite; Mc: microcline; Ap: apatite; Ti: titanite; Hb: hornblende.

plagioclase and clinopyroxene phenocrysts embedded in fine-grained groundmass of plagioclase, clinopyroxene, chlorite and glass (Fig. 6a). Plagioclase crystals show a preferred orientation due to magmatic flow showing trachytic texture. A few clinopyroxene crystals show alteration into chlorite along grain boundaries and fracture planes (Fig. 6b). Opaque minerals occur as small discrete grains within the fine-grained plagioclase and clinopyroxene groundmass (Fig. 6c).

4. Geochemistry

4.a. Methods

Thirteen representative samples of Tirit granitoids and eight samples of mafic dykes were analysed for major, trace and rare earth elements (REE) at the National Geophysical Research Institute (NGRI), Hyderabad, India. Major elements were determined by X-ray fluorescence (XRF) spectrometer on powder pellets using a Philips Model PW-2440 Spectrometer. United States Geological Survey (USGS) G-2 geological rock standard was used for calibration and quantitative estimation of chemical elements. Trace elements including REE and high-field-strength elements (HFSE) were determined by high-resolution inductively coupled plasma mass spectrometer (HR-ICP-MS). Reference materials from the Geological Survey of Japan (JB-2, JB-3, JB-1a) and USGS (BHVO-1, BCR-1, BIR-1) along with a couple of procedural blanks were also analysed, with the sample batches as controls on accuracy.

Whole-rock major elemental analyses of dykes were carried out by XRF spectrometery techniques. Trace elements including REE were determined by ICP-MS techniques at Wadia Institute of Himalayan Geology (WIHG), Dehradun, Uttarakhand, India.

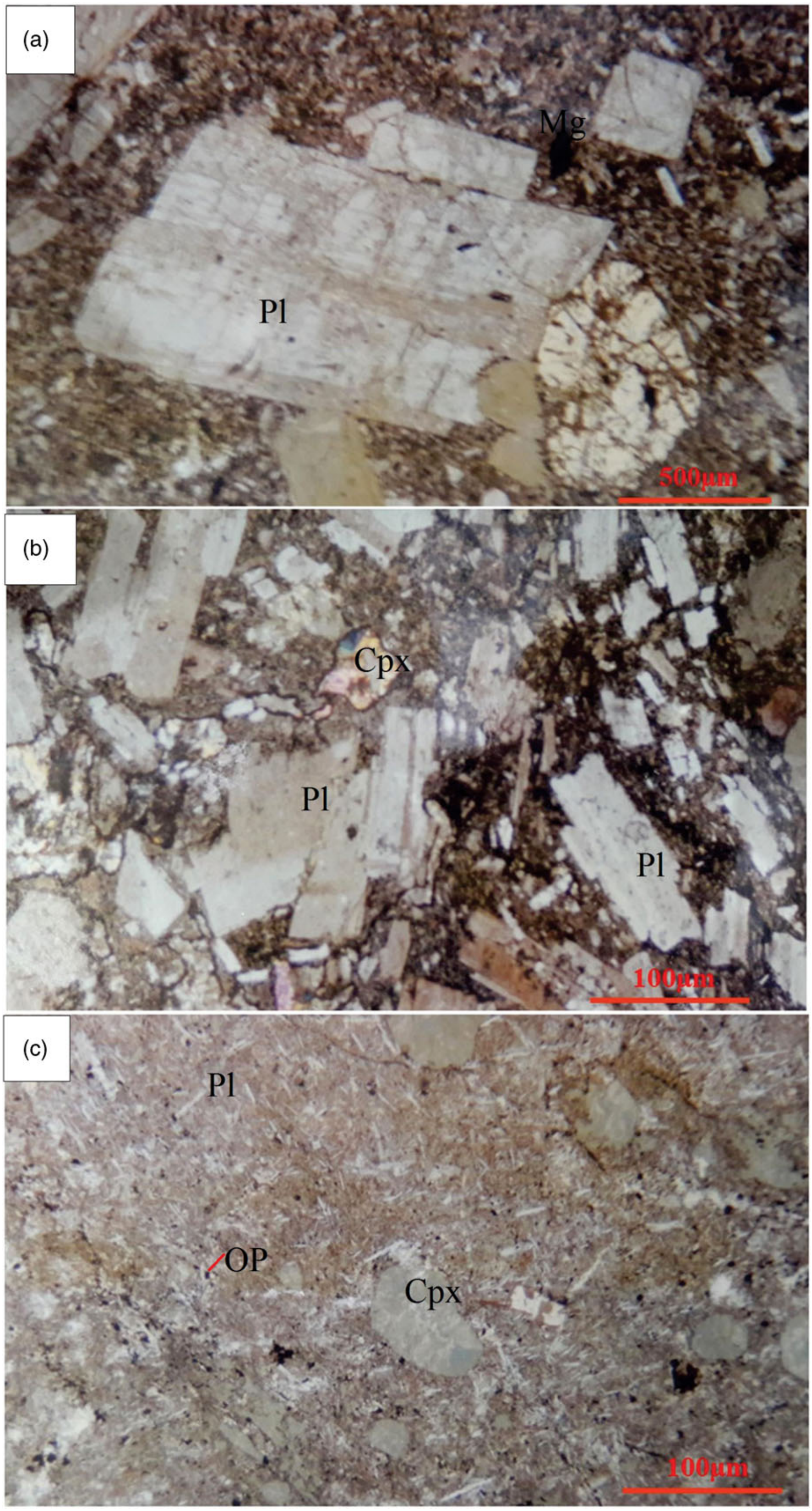

Fig. 6. (Colour online) Photomicrographs of Tirit dykes showing (a) plagioclase phenocrysts embedded in fine-grained groundmass of clinopyroxene, chlorite and glass (XPL); (b) plagioclase grains with a preferred orientation due to magmatic flow exhibiting trachytic texture (XPL); (c) opaque minerals within the fine-grained groundmass of plagioclase and clinopyroxene. Pl: plagioclase; Mg: magnetite; Op: opaques; Cpx: clinopyroxene.

4.b. Results and interpretation

4.b.1 Tirit granitoids

Geochemical data for the Tirit granitoids are provided in Supplementary Table S1, and CIPW norms in Table 1. The Tirit granitoids have a wide range of chemical compositions, with $SiO_2 = 50.91–72.11$ wt %, $TiO_2 = 0.21–1.23$ wt %, $Al_2O_3 = 11.42–14.00$ wt %, $MgO = 1.69–10.69$ wt % and $CaO = 3.24–9.31$ wt % (Supplementary Table S1). The high content of certain oxides like MgO and Al_2O_3 suggests the mafic components in the source region. Major elements exhibit linear trends against SiO_2, confirming the role of magmatic differentiation in their evolution. Harker Variation plots show a positive trend of SiO_2 with Na_2O and Al_2O_3 and negative trend with MgO, $FeO^{(t)}$, TiO_2 and P_2O_5 (Supplementary Fig. S1). The positive trend of Na_2O with silica reflects increasing modal plagioclase and K-feldspar. However, negative variation trends of MgO, TiO_2 and P_2O_5 indicate the fractional crystallization of hornblende, magnetite, titanite and apatite. Harker Variation trace element plots against SiO_2 show decreasing Ni, Ta, Pb and Sr but no correlation of Rb, Ba, Y and Zr (Supplementary Fig. S2), which may be due to variable amounts of minerals rich in these elements (Pearce & Norry, 1979). The Tirit granitoids fall within the granite, granodiorite and trondhjomite fields on a normative albite (ab) – anorthite (an) – orthoclase (or) plot (Fig. 7a); on the calc-alkaline differentiation trend on an AFM ternary plot (Fig. 7b); in the metaluminous field on A/CNK and A/NK plots (Fig. 7c); and are I-type on the Chappell & White (1974) plot (Fig. 7d). They show similar patterns on a bulk rock REE normalization to chondrite (Boynton, 1984), although with differences in abundance, showing considerable enrichment in the light REE (LREE; $(La/Sm)N = 2.20–6.53$) compared to the heavy REE (HREE; $Gd/Yb)N = 0.86–1.91$) (Fig. 8).

4.b.2. Tirit dykes

Geochemical data for the Tirit dykes are reported in Supplementary Table S2., and CIPW norms in Table 2. The dykes have a low but wide range of SiO_2 (48.95 to 57.49 %), are enriched in Al_2O_3 % (14.62 to 16.98 %), and have a markedly low TiO_2 content (0.64 to 1.11 %). MgO ranges from 5.77 to 10.31 wt % and total iron $FeO^{(t)}$ from 8.36 to 10.01 %. Na_2O ranges from 0.44 to 3.44 wt %. The K_2O ranges from 1.17 to 5.03 wt %.

During low-grade metamorphism, Zr (ppm) is considered to be relatively immobile (Winchester & Floyd, 1977; Macdonald *et al.* 1988). Hence, Zr can be used as a parameter for evaluating the elemental mobility and also to understand the differentiation/fractional crystallization of magma. In order to assess the fractional crystallization and also the mobility of major elements of Tirit dykes during the post-crystallization processes, these elements has been plotted against Zr. Most of the major elements including $FeO^{(t)}$, MgO, MnO, CaO and TiO_2 show a negative relationship with Zr. The SiO_2 wt %, Al_2O_3 and P_2O_5 wt % show a positive correlation with Zr. The normal negative and positive relationships probably indicate the primary magmatic characteristics for these major elements. However, the scattering of Na_2O wt % and K_2O wt % against the Zr indicate the mobile nature of Na_2O wt % and K_2O wt % during the post-crystallization processes (Supplementary Fig. S3). Binary plots of trace elements against Zr display positive trends with Nb, Th, Y and Sr and negative trends with Rb, Cr, Ni and U (Supplementary Fig. S4). In volcanic suites, the Nb/Y ratio is an indicator of alkalinity and the Zr/Ti ratio is a differentiation index (DI) (Pearce & Cann, 1973). When plotted together they define compositional fields (Winchester & Floyd, 1977), in which the Tirit dykes fall in the andesite – basaltic-andesite field (Fig. 9a). They are calc-alkaline on a ($Na_2O + K_2O$ versus SiO_2 plot (Fig. 9b). They are moderately enriched in LREE ($(La/Sm)N = 2.76–2.87$) and show relatively flat HREE ($(Gd/Yb)N = 1.76–2.05$) (Fig. 9c).

4.c. Petrogenesis

The Tirit granitoids show a continuous trend from mafic-rich (trondhjomite) to felsic-rich (granodiorite and quartz–diorite), with high Na_2O (av. 4.22) and low K_2O/Na_2O (av. 0.70), average molar A/CNK of 0.67 and A/NK of 1.36 (Table 1). Their metaluminous characteristics, high contents of TiO_2, Al_2O_3, MgO and high Sr and Ni indicate mafic components in the source region (Chappell & Stephens, 1988). Decrease in CaO % in rocks from low to high SiO_2 content is a result of crystal fractionation of plagioclase and calcic amphiboles. Zircon content and the regular pattern of decreasing P_2O_5 with increasing SiO_2 are characteristic of mafic low-temperature I-type granitoids (Chappell & White, 2001; Chappell *et al.*, 2004), whose petrogenesis is commonly attributed to variable interactions of mantle-derived mafic magmas with the continental crust, or to simple remagmatization of older crust with subsequent fractional crystallization and/or restite crystal fractionation (Chappell, 1996). The negative Eu/Eu* (0.59–0.91) anomaly in these granitoids suggests the removal of plagioclase feldspar from the source magma by fractional crystallization or residual feldspar in the source.

HFSE are least mobile, but show moderate degrees of fractional crystallization and are sensitive to partial melting and source inhomogeneities (Ahmad & Tarney, 1991). The ratios of Th/La, Th/Nb, Zr/Nb and Ce/Nd reveal the source characteristics and are higher in Tirit dykes than those of the primitive-mantle ratios (Sun & McDonough, 1989), indicating their derivation from enriched mantle sources (Table 2). The occasional higher Sr in these dykes suggests the fractionation of calcic plagioclase (Sun & McDonough, 1989). The moderate degrees of LREE enrichment, and flat HREE of the dykes (Fig. 9c) are typically shown by arc-related basalts and indicate an origin in a shallow (spinel–lherzolite) mantle (Murphy, 2007).

4.d. Tectonic setting

Maniar and Piccoli (1989) distinguished seven types of granitoids based on their tectonic setting. However, the Tirit granitoids show divergent settings. On the tectonic discrimination parameters R1 ($= [4Si - 11(Na + K) - 2(Fe + Ti)]$) and R2 ($= [6Ca + 2Mg + Al]$), most of the Tirit granitoids samples are in the post-collisional uplift, syn-collision and pre-plate collision fields (Fig. 10a). On the relative trace element Y + Nb versus Rb plot, however, they are in the Volcanic Arc Granites (VAG) field (Fig. 10b). Furthermore, on the Rb/Zr ratio against Nb and Y ppm plots of Brown *et al.* (1984), the samples are scattered and show no pattern (Fig. 10c).

Primitive-mantle-normalized spider diagrams for Tirit granitoids show negative anomalies of Nb, Ti, Zr, Ba and P along with positive anomalies of Th, U, K, Nd, Sm and Pb (Fig. 11), which suggests that they were derived from partial melting of juvenile crustal material possibly within a supra-subduction setting (Pearce *et al.* 1984; Qi *et al.* 2014). Fluids and melts derived from

Table 1. Tirit granitoids CIPW norms

Sample no.	PS3	PS7	TB3	TBS7	DM4	DM5	T9	T10	T11	T5	KS3	KS4	TB7
Q	12.91	15.27	11.12	10.8	33.66	31	15.91	12.85	12.02	16.29	0	0	12.93
Or	5.2	2.19	32.03	31.14	6.91	9.81	26.71	27.84	2.25	6.86	9.28	13.95	31.85
Ab	42.56	39.6	33.93	26.99	35.37	36.72	36.72	36.05	60.59	32.92	25.05	26.06	31.9
An	9.78	13.15	3.32	5.23	8.94	7.32	3.37	3.86	3.44	17.31	17.47	15.19	3.28
Di	16.67	23.86	9.46	9.67	7.31	8.86	9.48	11.37	15.83	7.04	23.27	21.68	10.69
Wo	0	0	0	0	0	0	0	0	2.02	0	0	0	0
Hy	7.9	1.92	5.5	10.58	3.58	2.64	3.19	3.61	0	13.25	7.64	7.04	4.92
Ol	0	0	0	0	0	0	0	0	0	0	9.94	7.19	0
Mt	4.93	1.48	5.83	7.35	5.66	5.25	4.55	4.55	1.87	8.58	13.66	12.76	6.24
Il	1.33	1.31	1.29	1.43	0.42	0.4	0.91	1.03	1.22	1.62	2.34	1.9	1.31
Hm	0	0.16	0	0	0	0	0	0	0	0	0	0	0
Ap	0.4	0.45	0.33	0.36	0.12	0.12	0.31	0.33	0.33	0.4	0.52	0.45	0.36
Other													
Eu/Eu*	0.88	0.77	0.68	0.86	0.82	0.82	0.62	0.67	0.6	0.73	0.91	0.85	0.59
(La/Sm)N	2.2	2.44	3.75	4.27	2.8	3.37	5.17	3.44	3.26	6.53	2.89	3.89	4.76
(Gd/Yb)N	1.91	1.57	1.29	1.63	0.86	0.94	1.26	1.28	1.33	1.66	1.4	1.24	1.39
A/CNK	0.61	0.52	0.74	0.73	0.77	0.74	0.74	0.71	0.58	0.79	0.52	0.56	0.72
A/NK	1.39	1.59	1.1	1.17	1.4	1.3	1.11	1.12	1.1	1.83	1.86	1.73	1.1

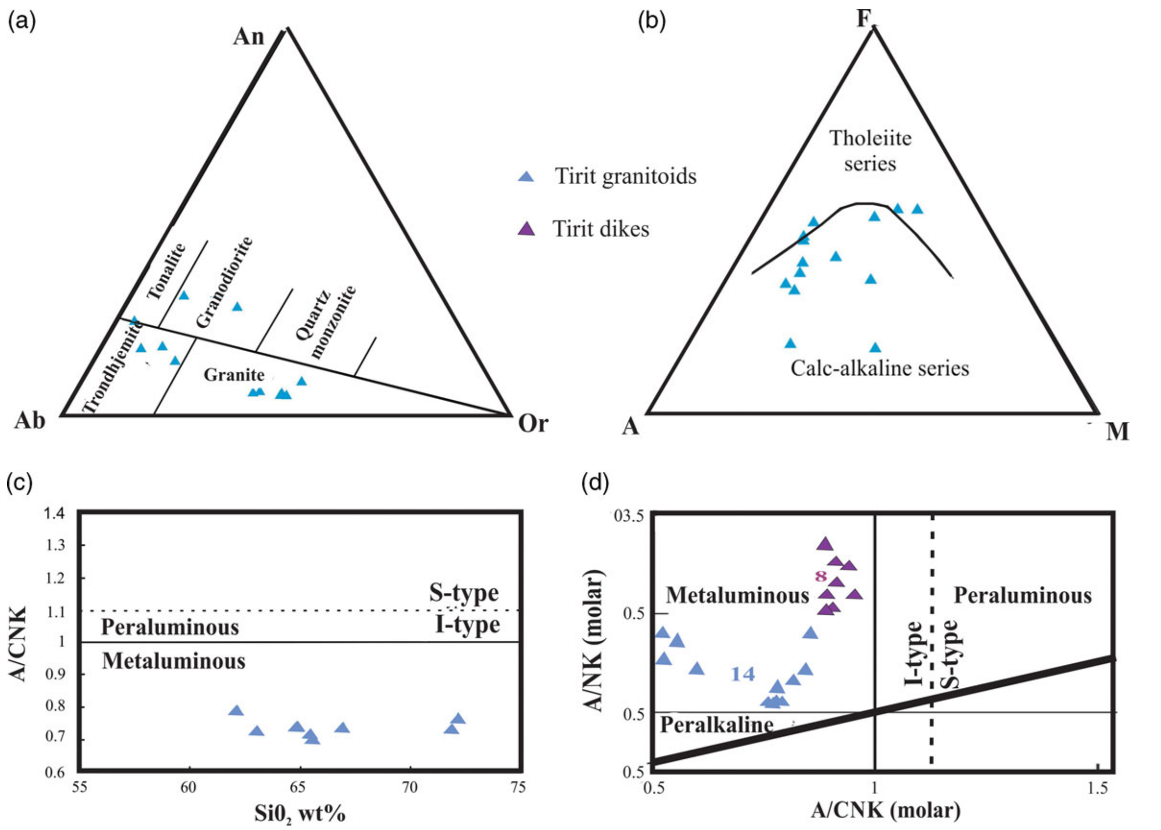

Fig. 7. (Colour online) Tirit granitoids: (a) An–Ab–Or classification diagram (after O'Connor, 1965); (b) AFM diagram (after Irvine & Baragar, 1971); (c) A/CNK versus SiO_2 wt % diagram (after White & Chappell, 1977); (d) molar A/CNK versus A/NK plots showing their metaluminous nature (after Shand, 1943).

https://doi.org/10.1017/S0016756823000134 Published online by Cambridge University Press

Table 2. Tirit dykes CIPW norms

Sample no.	SB R31	SB R32	SB R33	SB R34	SB R35	SB R36	SB R37	SB R38
Quartz	–	8.56	–	–	1.48	–	–	0.64
Orthoclase	7.74	11.82	29.73	6.91	24.35	9.99	11.35	6.74
Albite	26.57	27.25	3.72	26.23	11.08	29.11	29.02	24.96
Anorthite	21.93	24.91	28.17	22.55	28.29	21.21	20.6	25.85
hy	23.99	18.21	4.28	13.82	21.65	21.57	15.97	25.57
mt	3.57	2.6	3.91	3.74	3.38	3.35	3.36	3.26
il	2.03	1.67	1.82	2.11	1.67	1.79	1.84	1.61
ap	0.65	0.65	0.63	0.76	0.63	0.63	0.65	0.58
di	7.66	2.95	14.06	9.05	6.41	6.68	9.23	5.61
C	–	–	–	–	–	–	–	–
ol	2.76	–	13.09	11.03	–	2.41	5.21	–
ne	–	–	–	–	–	–	–	–
Other								
Plagioclase	An45	An48	An88	An46	An72	An42	An42	An51
(La/Sm)N	2.84	–	–	–	–	–	2.87	2.77
(Gd/Yb)N	2.05	–	–	–	–	–	1.79	1.77
Th/Nb	0.87	1.14	0.56	0.71	0.93	0.64	0.54	0.73
Zr/Nb	19.86	20.44	17.29	19.43	20.29	19.25	18.63	15.5
Ce/Nd	1.73	–	–	–	–	–	1.85	1.79
Th/La	0.27	–	–	–	–	–	0.24	0.31

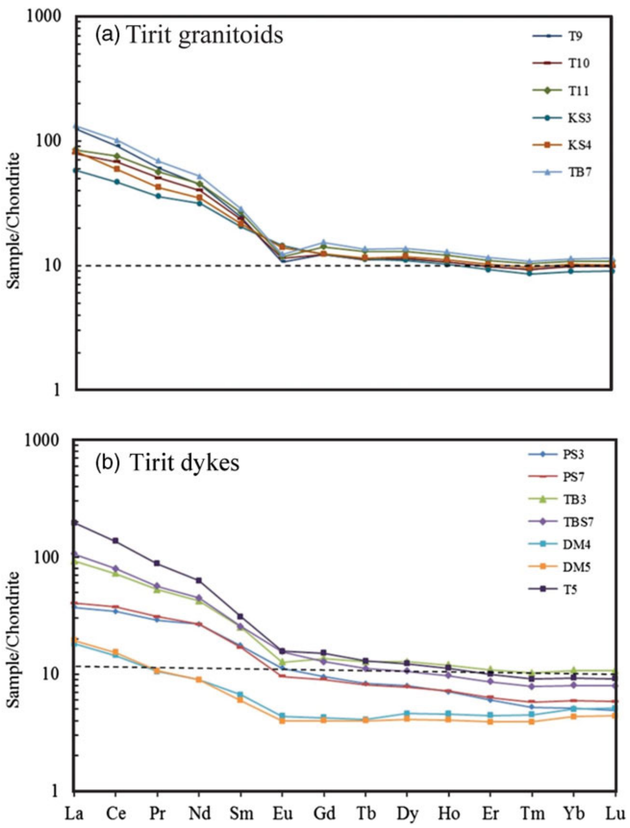

Fig. 8. (Colour online) Rare earth elements (REE) chondrite-normalized pattern diagrams of Tirit granitoids (a) and Tirit dykes (b). Chondrite values of Boynton (1984).

https://doi.org/10.1017/S0016756823000134 Published online by Cambridge University Press

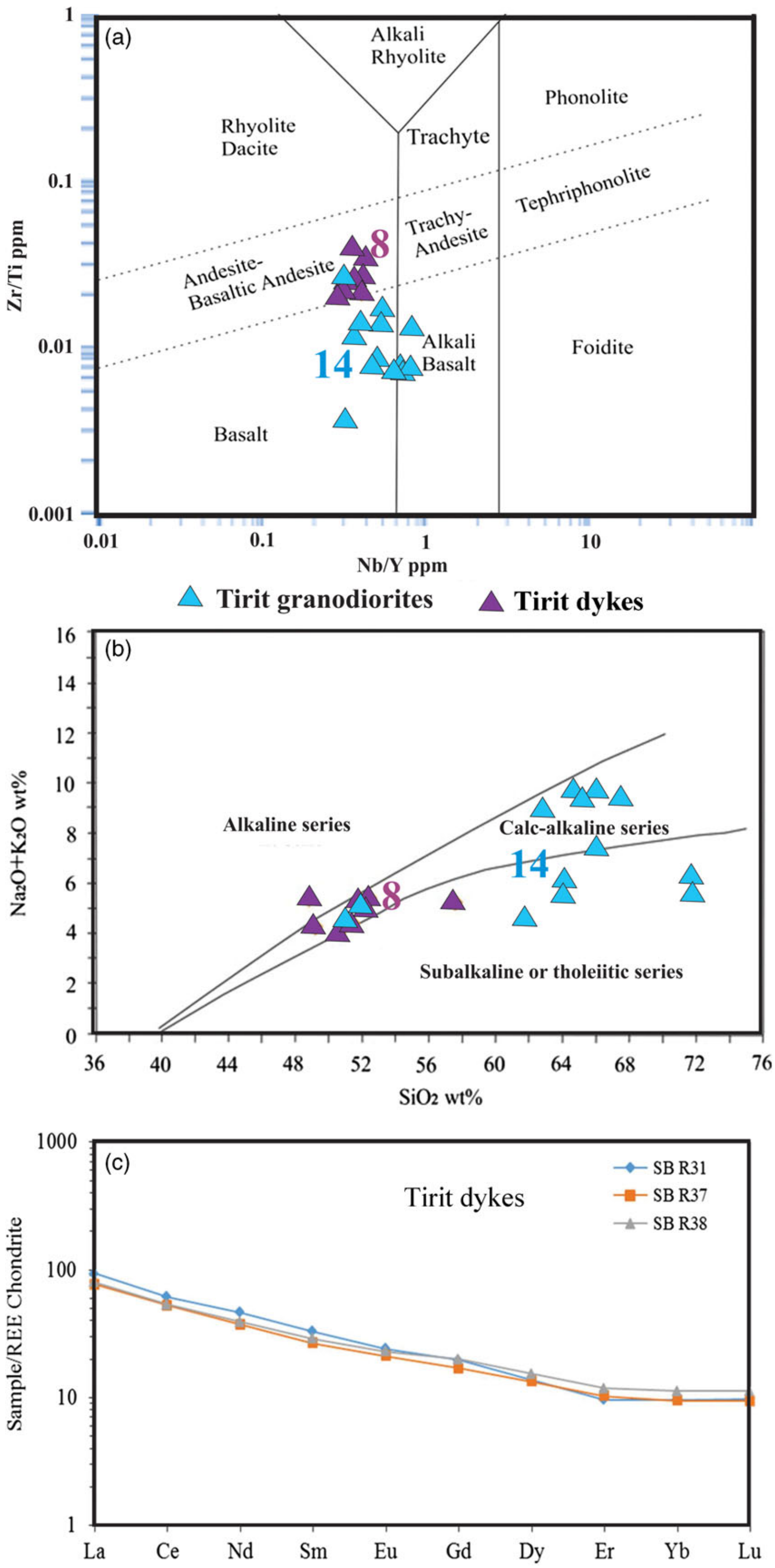

Fig. 9. (Colour online) (a) Zr/Ti versus Nb/Y plot on immobile elements classification diagram for Tirit granitoids and dykes showing andesite – basaltic-andesite composition (after Winchester & Floyd, 1977). (b) $Na_2O + K_2O$ wt % versus SiO_2 wt % plot for Tirit granitoids and dykes, showing their calc-alkaline nature (after Kuno, 1968). (c) Rare earth elements (REE) pattern for Tirit dykes showing enriched LREE and relatively depleted HREE (chondrite-normalizing values of Sun & McDonough, 1989).

https://doi.org/10.1017/S0016756823000134 Published online by Cambridge University Press

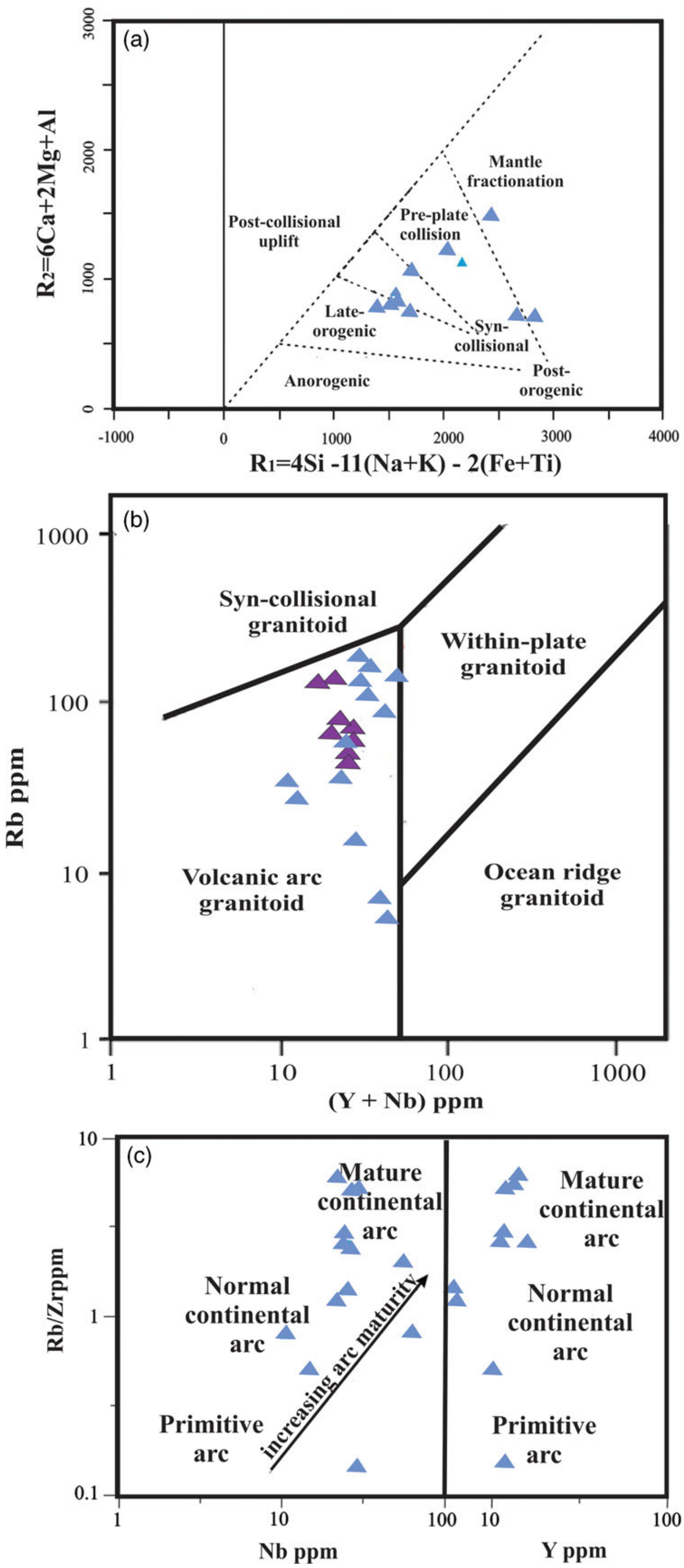

Fig. 10. (Colour online) (a) Multi-cationic R1 versus R2 tectonic discrimination diagram for Tirit granitoids of Nubra–Shyok Valley showing pre-plate collision and post-collision uplift of Tirit granitoids (after Batchelor & Bowden, 1985); (b) Rb versus Y + Nb tectonic discriminant diagrams for Tirit granitoids and dykes (after Pearce *et al*. 1984); (c) Rb/Zr versus Nb and Y for Tirit granitoids showing transitional nature (after Brown *et al*. 1984).

https://doi.org/10.1017/S0016756823000134 Published online by Cambridge University Press

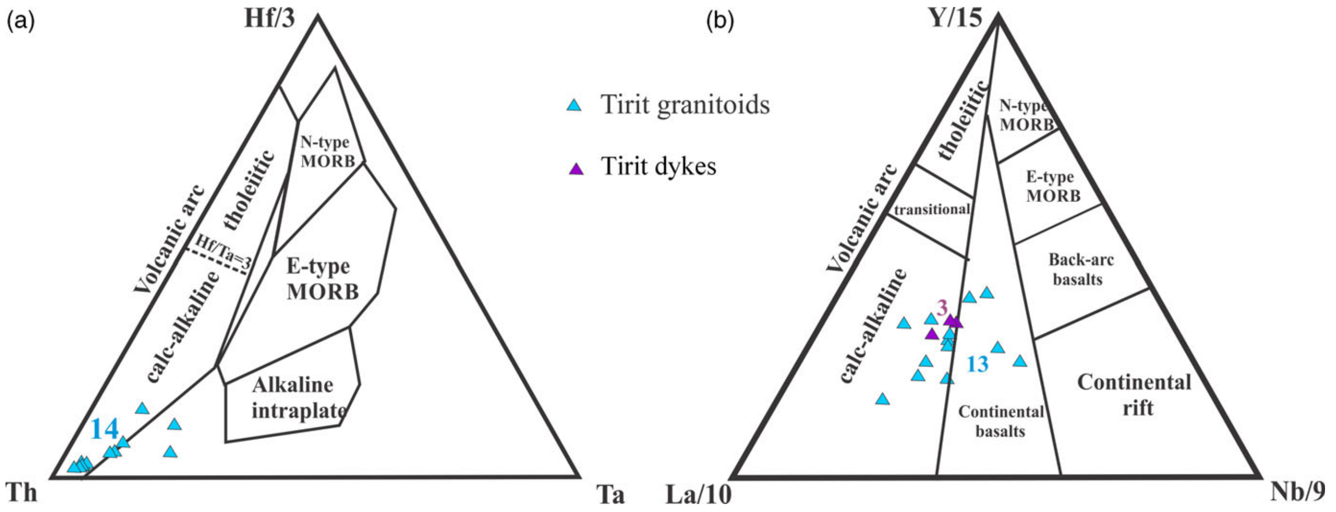

Fig. 11. (Colour online) (a) Hf–Tb–Ta plot of Tirit granitoids, showing dominantly in calc-alkaline field and extreme Hf and Ta depletion; (b) Y–La–Nb plot of Tirti granitoids and dykes showing dominantly calc-alkaline nature.

the subducted oceanic slab led to metasomatism of the upper mantle wedge and negative anomalies of Nb (Cox *et al.* 1979; Chappell, 1999). The positive anomalies in Pb and K, however, are attributed to metasomatism of mantle wedge by fluids derived from the subducted slab and/or contamination with continental crust (Kamber *et al.* 2002).

On the ternary 2Nb – Zr/4 – Y plot of Meschede (1986), the Tirit dykes scatter across several fields (Fig. 12a), while on the binary Zr/Y – Zr plot of Pearce (1983) they plot firmly in the continental arc basalts field, with higher Zr/Y than oceanic basalts (Fig. 12b). The primitive-mantle-normalized plot of the dyke elements is similar to the Tirit granitoid plot, and shows enrichment in U and Pb, and depletion in Nb and Ti (Fig. 13a), with the the negative Nb anomaly in both granitoids and dykes caused by subduction-related enrichment of lithospheric mantle (Kepezhinskas *et al.* 1997).

5. Geochronology

Previous U/Pb ion-microprobe ages from a tonalite at Tirit range from 66.8 ± 2.0 to 70.7 ± 0.8 Ma (11 spots; 6 slightly younger ages are considered altered) with a weighted mean of 68 + 1 Ma (Weinberg *et al.* 2000). A best-fit intercept U/Pb date from a granodiorite at Tirit gave 71.40 ± 0.36 Ma (Upadhyay, 2008); an Ar/Ar integrated total gas cooling age on hornblende from a diorite north of Khalsar was 73.6 ± 2.0 Ma, which is statistically the same as the age spectrum date of 73.1 ± 2.2 Ma (Weinberg *et al.* 2000); and an albite porphyroblast from a greenschist NW of Tirit gave a date of 65.4 ± 3.3 Ma, though abundant phengite inclusions may have affected the date (Thanh *et al.* 2010). Zircons from a granite at Hundar – supposedly from the Ladkah batholith, but probably from enclaves within it (Kumar, 2020) – gave a weighted mean average (of three dates) of 66.6 ± 2.1 Ma (Upadhyay *et al.* 2008). All errors have been increased, where necessary, from cited 1σ to 2σ, in keeping with normal practice, as 1σ gives an unacceptable 1-in-3 chance of being wrong, while 2σ gives a more acceptable 1-in-20 chance (Wyatt *et al.* 1998).

We analysed zircons in a tonalite (TB3) from Tirit Bridge (TB3) locality, using LA-ICP-MS with methods described in Liu & Stockli (2020) (Table 3; Fig. 13b). The most concordant zircon gives an age of 69.24 ± 0.96 Ma, with a lower intercept age for the 26 acceptable zircons of 64 ± 14 Ma, and MSWD = 4.6.

The dates are consistent with intrusion of the more mafic Tirit granitoids being somewhat older than the more felsic granitoids, spanning ~74 to 66 Ma. The dykes are younger than this.

6. Tectonic significance

The northward motion of India from the Mid Cretaceous to Eocene was accommodated by northward subduction of Neo-Tethys lithosphere along the ISZ and SSZ (Coward *et al.* 1986; Debon *et al.* 1987; Heuberger *et al.* 2007; Kumar *et al.* 2017), sporadically producing very large volumes of diversified granitoids. The Tirit granitoids were intruded during a relatively short episode of latest Cretaceous island arc development that is contemporary with the Spong island arc of the Indus suture zone to the south (Catlos *et al.* 2018) prior to the latest Cretaceous obduction of the Spongtang and other ophiolite nappes onto the northern Indian margin in the middle of the Tethys Ocean (Corfield *et al.* 2001; Gibbons *et al.* 2015). In that case a Palaeocene – early Eocene magmatic arc is required to obliterate the oceanic lithosphere between northern India and Asia, and this might be represented by the calc-alkaline, island arc plutonic bodies of the Leh pluton (60 ± 5 Ma), the Chang La pluton (57.6 ± 1.4 Ma to 53.4 ± 1.8 Ma) (Debon *et al.* 1987; Upadhyay *et al.* 2008) and the Palaeocene Ras Koh arc in SW Pakistan (Nicholson *et al.* 2010) (Fig. 14). The final 'hard' collision of India and Asia then occurred in the early Eocene between 50 and 45 Ma (Rex *et al.* 1988; Rolland, 2002; Upadhyay, 2008; Khan *et al.* 2009; Jain, 2014), following which further northward movement of the Indian Plate and compression and uplift formed the Himalaya (Fig. 15). The younger mafic dykes trending NW–SE in the Tirit granitoids may be related to the activity on the strike-slip Karakoram fault. Evaluating the complex and competing versions of this history, however, requires a more detailed (and expanded) study (Andjić *et al.* 2022).

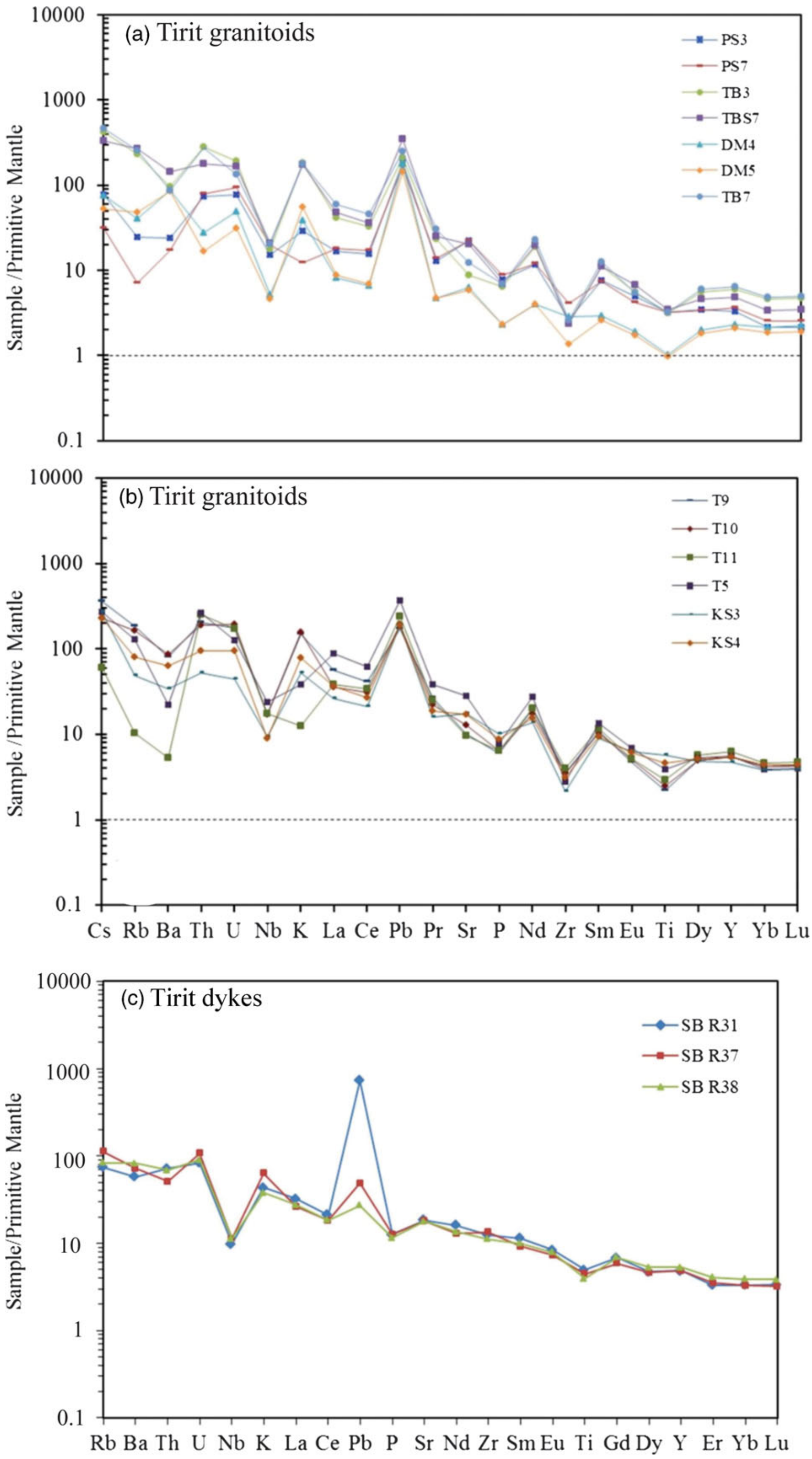

Fig. 12. (Colour online) Multi-element spider plots of Tirit granitoids and dykes showing negative anomalies of Rb, Ba, Nb, Pr, P, Zr, Ba and P along with positive anomalies of U, K, Pb, Nd and Sm (normalized values of Sun & McDonough, 1989).

Table 3. LA-ICP-MS geochronology, sample TB3 of Tirit granitoids

Grain no.	[U] (ppm)	U/Th	$^{207}Pb/^{235}U$	2σ error	$^{206}Pb/^{238}U$	2σ error	Age (Ma)	2σ error
TB3_2	347	0.78	0.0701	0.0056	0.0108	0.00023	69.2	1.5
TB3_3	172	0.91	0.0729	0.0050	0.0105	0.00022	67.5	1.4
TB3_4	313	0.88	0.0704	0.0029	0.0108	0.00015	69.39	0.99
TB3_6	245	0.82	0.0778	0.0036	0.0107	0.00019	68.5	1.2
TB3_8	244	0.74	0.0738	0.0034	0.0107	0.00018	68.5	1.2
TB3_9	395	2.98	0.0801	0.0039	0.0106	0.00018	68.2	1.1
TB3_10	971	2.52	0.0816	0.0048	0.0110	0.00041	70.5	2.6
TB3_12	403	0.64	0.0724	0.0034	0.0107	0.00022	68.5	1.4
TB3_13	587	0.88	0.0919	0.0059	0.0111	0.00026	DISC	DISC
TB3_14	497	0.86	0.0752	0.0029	0.0108	0.00015	69.24	0.96
TB3_15	361	0.88	0.0711	0.0030	0.0108	0.00022	68.9	1.4
TB3_16	312	0.79	0.0693	0.0030	0.0113	0.00021	72.3	1.3
TB3_18	635	0.69	0.0718	0.0034	0.0109	0.00021	69.7	1.3
TB3_19	810	1.13	0.0852	0.0053	0.0111	0.00040	DISC	DISC
TB3_20	229	0.62	0.0699	0.0038	0.0106	0.00019	67.7	1.2
TB3_21	494	0.80	0.0739	0.0042	0.0108	0.00022	69.5	1.4
TB3_23	610	1.25	0.0746	0.0050	0.0110	0.00021	70.7	1.3
TB3_24	279	0.74	0.0805	0.0041	0.0109	0.00021	69.6	1.3
TB3_25	182	0.93	0.0717	0.0047	0.0114	0.00022	72.7	1.4
TB3_27	193	0.80	0.0732	0.0046	0.0111	0.00023	70.8	1.4
TB3_28	234	1.10	0.081	0.0076	0.0104	0.00026	DISC	DISC
TB3_29	298	0.81	0.0768	0.0038	0.0106	0.00016	68.2	1
TB3_30	1090	0.93	0.0766	0.0026	0.0110	0.00018	70.5	1.2
TB3_31	940	1.07	0.078	0.0028	0.0114	0.00027	72.8	1.7

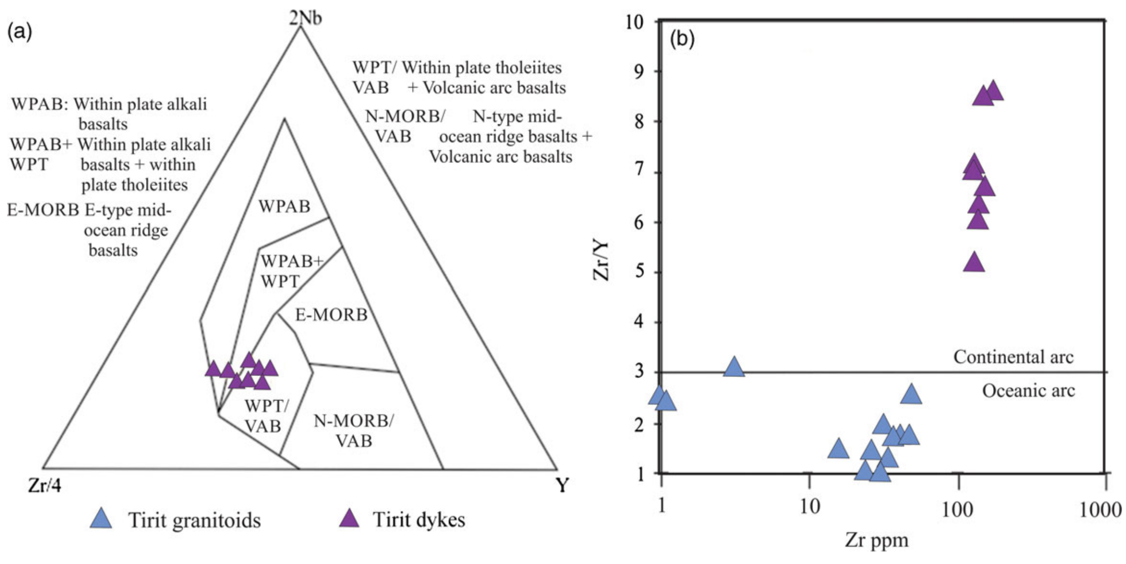

Fig. 13. (Colour online) (a) 2Nb – Zr/4 – Y ternary plot for Tirit dykes in dominantly volcanic arc basalt and within-plate tholeiite fields (after Pearce, 1983). (b) Zr (ppm) versus Zr/Y plot for Tirit granitoids and dykes: oceanic arc for granitoids, continental arc for dykes (after Pearce, 1983).

https://doi.org/10.1017/S0016756823000134 Published online by Cambridge University Press

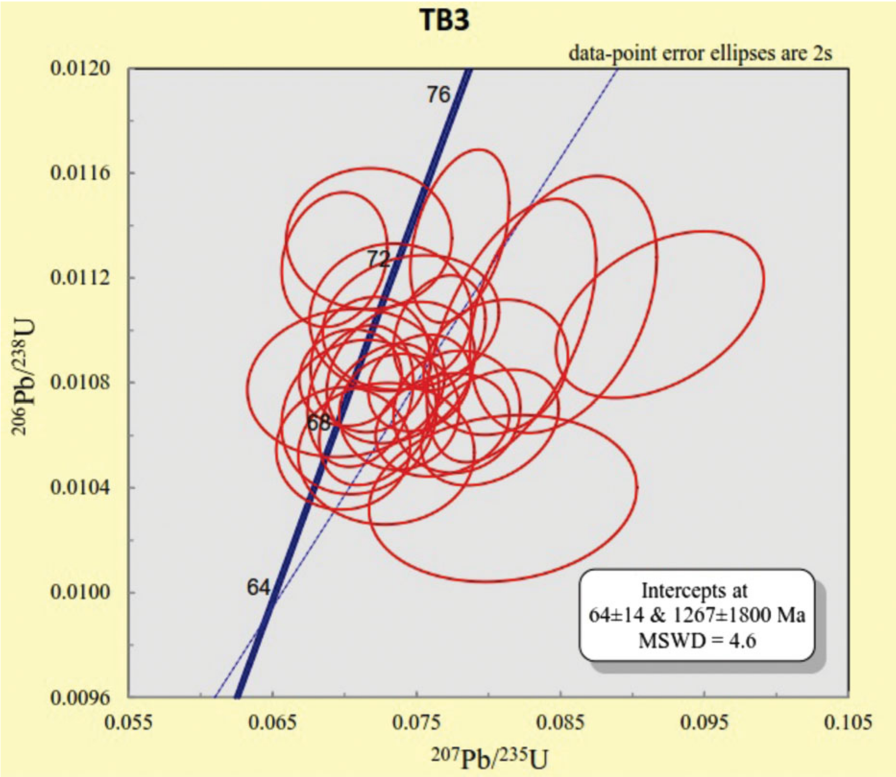

Fig. 14. (Colour online) Concordia $^{207}Pb/^{235}U$ versus $^{206}Pb/^{238}U$ diagram for zircons from TB3 sample of the Tirit granitoids.

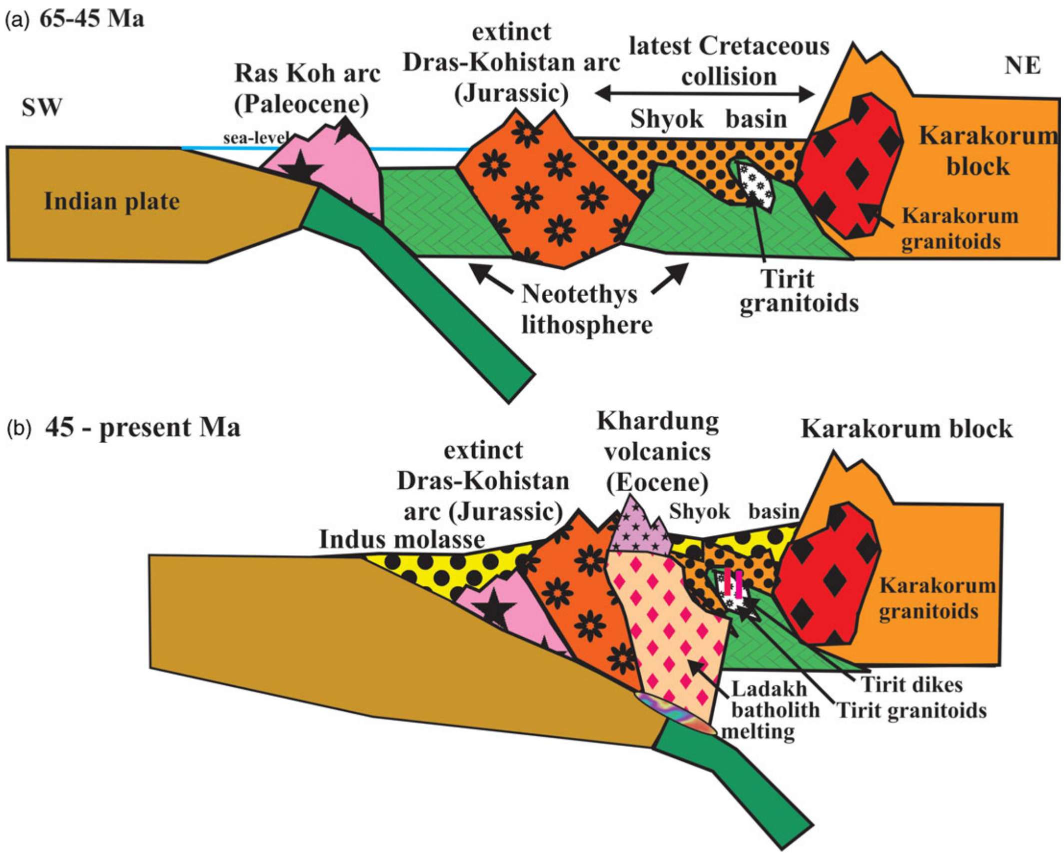

Fig. 15. (Colour online) Diagram showing (a) 65–45 Ma emplacement of Tirit granitoids during initial collision of extinct Ladakh arc with Karakoram Andean arc and development of Palaeocene arc to south, followed by (b) 45 Ma – present hard collision of India with Asia and partial melting of subducted Indian slab to give Ladakh batholith and associated volcanics with emplacement of the Tirit dykes.

https://doi.org/10.1017/S0016756823000134 Published online by Cambridge University Press

7. Conclusion

The integrated field, petrographical, geochemical and geochronological data indicate that the calc-alkaline Tirit granitoids were emplaced between ~71 and 58 Ma, during the later stages of an Upper Cretaceous to Palaeocene arc. They were further deformed during the India–Asia collision along the Indus Suture Zone around 45 Ma. The younger Tirit dykes, with high Th/La, Th/Nb, Zr/Nb and Ce/Nd ratios, have subducted components, inherited from the subcontinental mantle lithosphere in a post-collisional setting, and could also be related to the development of the NW–SE Karakoram fault.

Supplementary material. To view supplementary material for this article, please visit https://doi.org/10.1017/S0016756823000134

Acknowledgements. Nazia Kowser gratefully acknowledges the Department of Earth Science, University of Kashmir, Srinagar, J&K for providing laboratory facilities. The authors would also like to thank the director and scientists in charge of the analytical laboratories of the National Geophysical Research Institute (NGRI), Hyderabad, India, for their help throughout the analytical work. The authors express gratitude to the scientists of the (LA-ICP-MS laboratory at the Jackson School of Geosciences, University of Texas at Austin, who provided geochronological data for the present study. Yann Rolland did a comprehensive and very helpful review.

Declaration of interest. The authors declare none.

References

Ahmad T and Tarney J (1991) Geochemistry and petrogenesis of Garhwal volcanics: implications for evolution of the north Indian Lithosphere. *Precambrian Research* **50**, 69–88.

Allen TA and Chamberlain CP (1991) Metamorphic evidence for an inverted crustal section, with constraints on the Main Karakorum Thrust, Baltistan, Northern Pakistan. *Journal of Metamorphic Petrology* **9**, 403–18.

Andjić G, Zhou R, Jonell TN and Aitchison JC (2022) A single Dras-Kohistan-Ladakh arc revealed by volcaniclastic records. *Geochemistry, Geophysics, Geosystems* **23**, e2021GC010042. doi: 10.1029/2021GC010042.

Batchelor RA and Bowden P (1985) Petrogenetic interpretation of granitoid rock series using multicationic parameters. *Chemical Geology* **48**, 43–55. doi: 10.1016/0009-2541(85)90034-8.

Bhutani R, Pande K and Venkatesan TR (2009) ^{40}Ar-^{39}Ar dating of volcanic rocks of the Shyok suture zone in north-west Trans-Himalaya: implications for the post-collision evolution of the Shyok Suture Zone. *Journal of Asian Earth Sciences* **34**, 168–77.

Blair TC and McPherson JG (2009) Processes and forms of alluvial fans. In *Geomorphology of Desert Environments*, 2nd edn (eds AJ Parsons and AD Abrahams), pp. 413–67. Berlin: Springer Verlag. doi: 10.1007/978-1-4020-5719-9J.

Borneman NL, Hodges KV, Vansoest MC, Bohon W, Wartho J-A, Cronk SS and Ahmad T (2015) Age and structure of the Shyok suture in the Ladakh region of northwestern India: implications for slip on the Karakoram fault system, *Tectonics* **34**, 2011–33. doi: 10.1002/2015TC003933.

Boynton WV (1984) Cosmogeochemistry of the rare earth elements: meteorite studies. In *Rare Earth Element Geochemistry* (ed. P Henderson), pp. 63–114. Amsterdam: Elsevier.

Brookfield M and Gupta VJ (1984) Permian fossils from the Shyok melange, near Shigar, Baltistan, Pakistan. *Indian Geologists' Association, Bulletin* **17**, 39–44.

Brookfield ME, Chung S-L and Shellnutt JG (2017) Mid-Miocene (post 12 Ma) displacement along the central Karakoram fault zone in the Nubra valley, Ladakh, India from spot LA-ICPMS U/Pb zircon ages of granites. *Journal of the Geological Society of India* **89**, 231–9.

Brookfield ME and Reynolds PH (1981) Late Cretaceous emplacement of the Indus Suture Zone Ophiolitic Melanges and an Eocene-Oligocene magmatic arc on the northern edge of the Indian plate. *Earth and Planetary Science Letters* **55**, 157–62.

Brown GC, Thorpe RS and Webb PC (1984) The geochemical characteristics of granitoids arcs and comments on magma sources. *Journal of the Geological Society* **141**, 413–26.

Catlos E, Pease E, Dygert N, Brookfield M, Schwarz W, Bhutani R, Pande K and Schmitt A (2018) Nature, age, and emplacement of the Spongtang Ophiolite, Ladakh, NW India. *Journal of the Geological Society* **176**, 284–305. doi: 10.1144/jgs2018-085.

Chappell BW (1996) Compositional variation within granite suites of the Lachlan Fold Belt: its causes and implications for the physical state of granite magma. *Transactions of the Royal Society of Edinburgh: Earth Sciences* **87**, 159–70.

Chappell BW (1999) Aluminium saturation in I- and S-type granites and the characterization of fractionated haplogranites. *Lithos* **46**, 535–51.

Chappell BW and Stephens WE (1988) Origin of infracrustal (I-type) granite magmas. *Transactions of the Royal Society of Edinburgh: Earth and Environmental Science* **79**, 71–86.

Chappell BW and White AJR (1974) Two contrasting granite types. *Pacific Geology* **8**, 173–4.

Chappell BW and White AJR (2001) Two contrasting granite types: 25 years later. *Australian Journal of Earth Sciences* **48**, 489–99.

Chappell BW, White AJR, Williams IS and Wyborn D (2004) Low- and high-temperature granites. *Transactions of the Royal Society of Edinburgh: Earth and Environmental Science* **95**, 125–40.

Corfield R, Searle M and Pedersen R (2001) Tectonic setting, origin, and obduction history of the Spongtang Ophiolite, Ladakh Himalaya, NW India. *The Journal of Geology* **109**, 715–36. doi: 10.1086/323191.

Coward MP, Windley BF, Broughton R, Luff IW, Petterson MG, Pudsey C, Rex D and Khan MA (1986) Collision tectonics in the NW Himalayas. In *Collision Tectonics* (eds MP Coward and A Ries), pp. 203–19. Geological Society of London, Special Publication no.19.

Cox KG, Bell JD and Pankhurst RJ (1979) *The Interpretation of Igneous Rocks*. London: George Allen & Unwin, 450 pp.

Debon F and Khan NA (1996) Alkaline orogenic plutonism in the Karakoram batholith: the Upper Cretaceous Koz Sar complex (Karamber valley, N. Pakistan). *Geodinamica Acta* **9**, 145–60.

Debon F, Le Fort P, Dautel D, Sonet J and Zimmermann JL (1987) Granites of western Karakoram and northern Kohistan (Pakistan): a composite Mid-Cretaceous to upper Cenozoic magmatism. *Lithos* **20**, 19–40.

Dewey JF (1977) Suture zone complexities: a review. *Tectonophysics* **40**, 53–67. doi: 10.1016/0040-1951(77)90029-4.

Dewey JF (2005) Orogeny can be very short. *Proceedings of the National Academy of Sciences* **102**, 15286–93.

Draut AE and Clift PD (2013) Differential preservation in the geologic record of intraoceanic arc sedimentary and tectonic processes. *Earth-Science Reviews* **116**, 57–84.

Dunlap WJ and Wysoczanski R (2002) Thermal evidence for early Cretaceous metamorphism in the Shyok Suture Zone and age of the Khardung volcanic rocks, Ladakh, India. *Journal of Asian Earth Sciences* **20**, 481–90.

Ehiro M, Kojima S, Sato T, Ahmad T and Ohtani T (2007) Discovery of Jurassic ammonoids from the Shyok suture zone to the northeast of Chang La Pass, Ladakh, northwest India and its tectonic significance. *Island Arc* **16**, 124–32. doi: 10.1111/j.1440-1738.2007.00562.x.

Frassi C, Pandolfi L, Marroni M, Göncüoğlu MC, Ellero A, Ottria G and Sayit K (2016) Insights in the Intra-Pontide Suture Zone in the Tosya-Kastamonu area, Northern Turkey. *Journal of Maps* **12**, 211–19.

Gaetani M (1997) The Karakorum Block in Central Asia, from Ordovician to Cretaceous. *Sedimentary Geology* **109**, 339–59.

Gansser A (1977) The great suture zone between Himalaya and Tibet, a preliminary account. In *Himalaya – sciences de la terra, Colloques International, 7–10 December 1976*, pp. 181–92. Editions du Centre National de la Researche Scientifique, Paris, no. 268.

Gibbons A, Zahirovic S, Müller D, Whittaker J and Vadakkeyakath Y (2015) A tectonic model reconciling evidence for the collisions between India, Eurasia and intra-oceanic arcs of the central-eastern Tethys. *Gondwana Research* **28**, 451–92. doi: 10.1016/j.gr.2015.01.001.

Hébert R, Bezard R, Guilmette C, Dostal J, Wang CS and Liu ZF (2012) The Indus–Yarlung Zangbo ophiolites from Nanga Parbat to Namche Barwa syntaxes, southern Tibet: first synthesis of petrology, geochemistry, and geochronology with incidences on geodynamic reconstructions of Neo-Tethys. *Gondwana Research* **22**, 377–97. doi: 10.1016/j.gr.2011.10.013.

Heri AR, Aitchison JC, King JA and Villa IM (2015) Geochronology and isotope geochemistry of Eocene dykes intruding the Ladakh Batholith. *Lithos* **212–215**, 111–21. doi: 10.1016/j.lithos.2014.11.001.

Heuberger S, Schaltegger U, Burg JP, Villa IM, Frank M, Dawood H, Hussain S and Zanchi A (2007) Age and isotopic constraints on magmatism along the Karakoram-Kohistan Suture Zone, NW Pakistan: evidence for subduction and continued convergence after India-Asia collision. *Swiss Journal of Geosciences* **100**, 85–107.

Horton F and Leech ML (2013) Age and origin of granites in the Karakoram shear zone and Greater Himalaya Sequence, NW India. *Lithosphere* **5**, 300–20. doi: 10.1130/L213.1.

Irvine TN and Baragar WRA (1971) A guide to the chemical classification of the common volcanic rocks. *Canadian Journal of Earth Sciences* **8**, 523–48. doi: 10.1139/e71-055.

Jain AK (2014) When did India–Asia collide and make the Himalaya? *Current Science* **106**, 254–66.

Juyal KP (2006) Foraminiferal biostratigraphy of the Early Cretaceous Hundiri Formation, lower Shyok area, eastern Karakorum, India. *Current Science* **91**, 1096–104.

Kamber BS, Ewart A, Collerson KD, Bruce MC and McDonald GA (2002) Fluid-mobile trace element constraints on the role of slab melting and implications for Archaean crustal growth models. *Contributions to Mineralogy and Petrology* **144**, 38–56.

Kassi AM, Khan AS and Kasi AK (2007) Newly proposed Cretaceous-Palaeocene lithostratigraphy of the Ispikan-Wakai area, southwestern Makran, Pakistan. *Journal of Himalayan Earth Sciences* **40**, 25–31.

Kepezhinskas P, McDermott F, Defant MJ, Hochstaedter A, Drummond MS, Hawkesworth CJ and Bellon H (1997) Trace element and Sr and Nd and Pb isotopic constraints on a three-component model of Kamchatka Arc petrogenesis. *Geochimica et Cosmochimica Acta* **61**, 577–600.

Khan S, Walker J, Hall S, Burke K, Shah M and Stockli L (2009) Did Kohistan-Ladakh island arc collide first with India? *Geological Society of America Bulletin* **121**, 366–84. doi: 10.1130/B26348.1.

Kumar S (2010) Mafic to hybrid microgranular enclaves in the Ladakh batholith, northwest Himalaya: implications on calc-alkaline magma chamber processes. *Journal of the Geological Society of India* **76**, 5–25. doi: 10.1007/s12594-010-0080-2.

Kumar S (2020) Schedule of mafic to hybrid magma injections into crystallizing felsic magma chambers and resultant geometry of enclaves in granites: new field and petrographic observations from Ladakh Batholith, Trans-Himalaya, India. *Frontiers in Earth Science*, 1–14. doi: 10.3389/feart.2020.551097.

Kumar S, Bora S and Sharma UK (2016) Geological appraisal of Ladakh and Tirit granitoids in the Indus-Shyok Suture zones of Northwest Himalaya, India. *Journal of the Geological Society of India* **87**, 737–46.

Kuno H (1968) Differentiation of basalt magmas. In *Basalts: The Poldervaart Treatise on Rocks of Basaltic Composition* (eds H Hess and A Poldervaart), pp. 623–88. New York: Interscience Publishers.

Lakhan N, Singh AK, Singh BP, Sen K, Singh MR, Khogenkumar S, Singhal S and Oinam G (2020) Zircon U–Pb geochronology, mineral and whole-rock geochemistry of the Khardung volcanics, Ladakh Himalaya, India: implications for Late Cretaceous to Palaeogene continental arc magmatism. *Geological Journal* **55**, 3297–320.

Liu D, Li H, Sun Z, Cao Y, Wang L and Pan J (2017) Cenozoic Episodic uplift and kinematic evolution between the Pamir and southwestern Tien Shan. *Tectonophysics* **712–713**, 438–54. doi: 10.1016/j.tecto.2017.06.009.

Liu L and Stockli D (2020) U-Pb ages of detrital zircons in Lower Permian sandstone and siltstone of the Permian Basin, west Texas, USA: evidence of dominant Gondwanan and peri-Gondwanan sediment input to Laurentia. *Geological Society of America Bulletin* **132**, 245–62. doi: 10.1130/B35119.1.

Macdonald R, Wilson L, Thorpe RS and Martin A (1988) Emplacement of the Cleveland dyke: evidence from geochemistry, mineralogy and physical modelling. *Journal of Petrology* **29**, 559–83.

Maniar PD and Piccoli PM (1989) Tectonic discrimination of granitoids. *Geological Society of America Bulletin* **101**, 635–46.

Matsumaru K, Ehiro M and Kojima S (2006) On Orbitolina (Foraminiferida) from the Shyok suture zone, Ladakh, NW India. *Journal of the Palaeontological Society of India* **51**, 43–9.

Meschede M (1986) A method of discriminating between different types of mid-ocean ridge basalts and continental tholeiites with the Nb-Zr-Y diagram. *Chemical Geology* **56**, 207–18.

Murphy MA (2007) Isotopic characteristics of the Gurla Mandhata metamorphic core complex: implications for the architecture of the Himalayan orogen. *Geology* **35**, 983–6.

Nicholson KN, Khan M and Mahmood K (2010). Geochemistry of the Chagai–Raskoh arc, Pakistan: complex arc dynamics spanning the Cretaceous to the Quaternary. *Lithos* **118**, 338–48. doi: 10.1016/j.lithos.2010.05.008.

O'Connor JT (1965) A classification for quartz-rich igneous rocks based on feldspar ratios. *United States Geological Survey Professional Paper* **525-B**, 79–84.

Parsons AJ, Hosseini K, Palin RM and Sigloch K (2020) Geological, geophysical and plate kinematic constraints for models of the India-Asia collision and the post-Triassic central Tethys oceans. *Earth-Science Reviews* **208**, 103084. doi: 10.1016/j.earscirev.2020.103084.

Pearce JA (1983) Role of the sub-continental lithosphere in magma genesis at active continental margin. In *Continental Basalt and Mantle Xenoliths* (eds WCJ Hawkes and MJ Norry), pp. 230–49. Nantwich: Shiva Publications.

Pearce JA and Cann JR (1973) Tectonic setting of basic volcanic rocks determined by using trace element analysis. *Earth and Planetary Science Letters* **19**, 290–300.

Pearce JA, Harris NBW and Tindle AG (1984) Trace element discrimination diagrams for the tectonic interpretation of granitic rocks. *Journal of Petrology* **25**, 956–83.

Pearce JA and Norry MJ (1979) Petrogenetic implications of Ti, Zr, Y and Nb variations in volcanic rocks. *Contributions to Mineralogy and Petrology* **69**, 33–47.

Petterson MP and Windley BF (1985) Rb-Sr dating of the Kohistan arc-batholith in the Trans-Himalaya of north Pakistan, and tectonic implications. *Earth and Planetary Science Letters* **74**, 45–57.

Pudsey C (1986) The Northern Suture, Pakistan: margin of a cretaceous island arc. *Geological Magazine* **123**, 405–23. doi: 10.1017/S0016756800033501.

Pundir S, Adlakha V, Kumar S and Singhal S (2020) Closure of India–Asia collision margin along the Shyok Suture Zone in the eastern Karakoram: new geochemical and zircon U–Pb geochronological observations. *Geological Magazine* **157**, 1451–72. doi: 10.1017/S0016756819001547.

Qi X, Luhua Z, Grimmer J and Hu Z (2014) Tracing the Transhimalayan magmatic belt and the Lhasa block southward using zircon U–Pb, Lu–Hf isotopic and geochemical data: Cretaceous – Cenozoic granitoids in the Tengchong block, Yunnan, China. *Journal of Asian Earth Sciences* **110**, 170–88. doi: 10.1016/j.jseaes.2014.07.019.

Rai H (1982) Geological evidence against the Shyok Palaeo-suture, Ladakh Himalaya. *Nature* **297**, 142–3.

Rai H (1983) Geology of the Nubra valley and its significance on the evolution of the Ladakh Himalaya. In *Geology of Indus Suture Zone of Ladakh* (eds VC Thakur and KK Sharma), pp. 79–91. Dehradun: Wadia Institute of Himalayan Geology.

Rao DR and Rai H (2009) Geochemical studies of granitoids from Shyok Tectonic Zone of Khardung-Panamik Section, Ladakh, India. *Journal of the Geological Society of India* **73**, 553–66.

Raz U and Honegger K (1989) Magmatic and tectonic evolution of the Ladakh Block from field studies. *Tectonophysics* **161**, 107–18. doi: 10.1016/0040-1951(89)90306-5.

Rehman HU, Seno T, Yamamoto H and Khan T (2011) Timing of collision of the Kohistan-Ladakh Arc with India and Asia: debate. *Island Arc* **20**, 308–28. doi: 10.1111/j.1440-1738.2011.00774.x.

Reuber I (1990) Les ophiolites de la Shyok dans l'Himalaya du Ladakh: reliques de la plaque océanique de la Tethys surmontée d'un arc volcano-sédimentaire daté du Crétacé moyen. *Comptes rendus de l'Académie des sciences, Série II* **310**, 1255–62.

Rex, AJ, Searle, MP, Tirrul R, Crawford, MB, Prior, DJ, Rex, DC and Barnicoat, A. (1988) The geochemical and tectonic evolution of the central Karakoram, North Pakistan. *Philosophical Transactions of the Royal Society* **A326**, 229–55. doi: 10.1098/rsta.1988.0086.

Reynolds P, Brookfield ME and McNutt R (1983). The age and nature of Mesozoic-Tertiary magmatism across the Indus Suture Zone in Kashmir and Ladakh (N. W. India and Pakistan). *Geologische Rundschau* **72**, 981–1003. doi: 10.1007/BF01848351.

Robertson AHF and Collins AS (2002) Shyok Suture Zone, N. Pakistan: late Mesozoic tertiary evolution of a critical suture separating the oceanic Ladakh Arc from the Asian continental margin. *Journal of Asian Earth Sciences* **20**, 309–51.

Rolland Y (2002) From intra-oceanic convergence to post-collisional evolution: the India-Asia convergence in NW Himalaya, from Cretaceous to present. *Journal of The Virtual Explorer* **8**, 183–205. doi: 10.3809/jvirtex.2002.00052.

Rolland Y, Mahéo G, Guillot S and Pêcher A (2001) Tectono-metamorphic evolution of the Karakorum Metamorphic complex (Dassu–Askole area, NE Pakistan): exhumation of mid-crustal HT–MP gneisses in a convergent context. *Journal of Metamorphic Geology* **19**, 717–37.

Rolland Y, Mahéo G, Pecher A and Villa IM (2009) Syn-kinematic emplacement of the Pangong metamorphic and magmatic complex along the Karakorum Fault (N Ladakh). *Journal of Asian Earth Sciences* **34**, 10–25.

Rolland Y, Pecher A and Picard C (2000) Middle Cretaceous back-arc formation and arc evolution along the Asian margin: the Shyok Suture Zone in northern Ladakh (NW Himalaya). *Tectonophysics* **325**, 145–73.

Rolland Y, Picard C, Pêcher A, Carrio E, Sheppard SM, Oddone M and Villa IM (2002a) Presence and geodynamic significance of Cambro-Ordovician series of SE Karakoram (N Pakistan). *Geodinamica Acta* **15**, 1–21.

Rolland Y, Picard C, Pecher A, Lapierre H, Bosch D and Keller F (2002b) The Cretaceous Ladakh arc of NW Himalaya: slab melting and melt–mantle interaction during fast northward drift of Indian Plate. *Chemical Geology* **182**, 139–78.

Rolland Y, Villa IM, Guillot S, Mahéo G and Pêcher A (2006) Evidence for pre-Cretaceous history and partial Neogene (19–9 Ma) reequilibration in the Karakorum (NW Himalayan Syntaxis) from ^{40}Ar–^{39}Ar amphibole dating. *Journal of Asian Earth Sciences* **27**, 371–91.

Saktura WM, Buckman S, Aitchison JC and Zhou R (2021a) Paleogene magmatic flex and flux in the Ladakh Arc, NW Himalaya: chronostratigraphy of the Khardung Formation. *Lithos* **388**, 106053. doi: 10.1016/j.lithos.2021.106053.

Saktura WM, Buckman S, Nutman AP and Bennett VC (2021b) Late Jurassic Changmar Complex from the Shyok ophiolite, NW Himalaya: a prelude to the Ladakh Arc. *Geological Magazine* **158**, 239–60. doi: 10.1017/S0016756820000400.

Schärer U, Copeland P, Harrison TM and Searle MP (1990) Age, cooling history, and origin of post-collisional leucogranites in the Karakoram Batholith: a multi-system isotope study. *The Journal of Geology* **98**, 233–51. doi: 10.1086/629395.

Schwab M, Ratschbacher L, Siebel W, Mcwilliams M, Minaev V, Lutkov V, Chen F, Stanek K, Nelson B, Frisch W and Wooden JL (2004) Assembly of the Pamirs: age and origin of magmatic belts from the southern Tien Shan to the southern Pamirs and their relation to Tibet. *Tectonics* **23**, TC4002. doi: 10.1029/2003TC0015.

Shand SJ (1943) *Eruptive Rocks: Their Genesis Composition, Classification, and Their Relation to Ore Deposits with a Chapter on Meteorites*. New York: John Wiley and Sons, 444 pp.

Shellnutt J, Lee T-Y, Brookfield M and Chung S-L (2014) Correlation between magmatism of the Ladakh Batholith and plate convergence rates during the India-Eurasia collision. *Gondwana Research* **26**, 1051–9. doi: 10.1016/j.gr.2013.09.006.

Shroder JF, Eqrar N, Waizy H, Ahmadi H and Weihs B (2021) Review of the geology of Afghanistan and its water resources. *International Geology Review* **64**, 1009–31. doi: 10.1080/00206814.2021.1904297.

Sinha AK, Rai H, Upadhyay R and Chandra R (1999) Contribution to the geology of the eastern Karakoram, India. *Geological Society of America Special Paper* 328, 33–44.

Sivaprabha S, Bhat IM, Ahmad T, Tanaka T, Balakrishnan S, Asahara Y and Mukhopadhyay D (2022) Geochemical analysis of magmatic rocks from Shyok Suture Zone (SSZ) Trans-Himalaya, NW India: insights for geodynamic evolution of the terrane. *Lithos* **410–411**, 106594. doi: 10.1016/j.lithos.2022.106594.

Srimal N (1986) India-Asia collision: implications from the geology of the eastern Karakoram. *Geology* **14**, 523–7.

Stern RJ, Reagan M, Ishizuka O, Ohara Y and Whattam S (2012) To understand subduction initiation, study forearc crust; to understand forearc crust, study ophiolites. *Lithosphere* **4**, 469–83.

St-Onge MR, Rayner N and Searle MP (2010) Zircon age determinations for the Ladakh Batholith at Chumathang (Northwest India): implications for the age of the India–Asia collision in the Ladakh Himalaya. *Tectonophysics* **495**, 171–83.

Sun SS and McDonough WF (1989) Chemical and isotopic systematics of oceanic basalts: implications for mantle composition and processes. In *Magmatism in the Ocean Basins* (eds AD Saunders and MJ Norry), pp. 313–45. Geological Society of London, Special Publication no. 42.

Thakur VC and Misra DK (1984) Tectonic framework of Indus and Shyok Suture Zones in eastern Ladakh, NW Himalaya. *Tectonophysics* **101**, 207–20.

Thanh NX, Itaya T, Ahmad T, Kojima S, Ohtani T and Ehir M (2010) Mineral chemistry and K-Ar ages of plutons across the Karakoram fault in the Shyok-Nubra confluence of northern Ladakh Himalaya, India. *Gondwana Research* **17**, 180–8.

Thanh NX, Rajesh VJ, Itaya T, Windley B, Kwon S, Park C-S, Ngac D, Liem T and Nam V (2012) A Cretaceous forearc ophiolite in the Shyok suture zone, Ladakh, NW India: implications for the tectonic evolution of the Northwest Himalaya. *Lithos* **155**, 81–93. doi: 10.1016/j.lithos.2012.08.016.

Upadhyay R (2002) Stratigraphy and tectonics of Ladakh, eastern Karakoram, western Tibet and western Kun Lun. *Journal of the Geological Society of India* **59**, 447–67.

Upadhyay R (2008) Implications of U-Pb zircon age of the Tirit Granitoids on the closure of the Shyok Suture Zone, northern Ladakh, India. *Current Science* **94**, 1635–9.

Upadhyay R (2009) U-Pb zircon age for a granite intrusion within the Shyok Suture Zone, Saltoro Hills, northern Ladakh. *Current Science* **97**, 1234–8.

Upadhyay R (2014) Palaeogeographic significance of "Yasin-type" rudist and orbitolinid fauna of the Shyok Suture Zone, Saltoro Hills, northern Ladakh, India. *Current Science* **106**, 223–8.

Upadhyay R, Frisch W and Siebel W (2008) Tectonic implications of new U-Pb zircon ages of the Ladakh batholith, Indus suture zone, northwest Himalaya, India. *Terra Nova* **20**, 309–17.

Upadhyay R, Gautam S and Awatar R (2014) Discovery of an entrapped early Permian (ca. 299 Ma) Peri-Gondwanic sliver in the Cretaceous Shyok Suture of Northern Ladakh, India: diverse implications. *GSA Today* **32**, 6. doi: 10.1130/GSATG481A.1.

Upadhyay R, Sinha AK, Chandra R and Rai H (1999) Tectonic and magmatic evolution of the eastern Karakoram, India. *Geodynamica Acta* **12**, 341–58.

Wallis D and Searle MP (2019) Spatial and temporal distributions of deformation in strike-slip faults: the Karakoram Fault in the India-Asia Collision Zone. In *Transform Plate Boundaries and Fracture Zones* (ed. JC Duarte), pp. 271–300. Amsterdam: Elsevier. doi: 10.1016/B978-0-12-812064-4.00011-6.

Weinberg RF, Dunlap WJ and Whitehouse M (2000) New field, structural and geochronological data from the Shyok and Nubra valleys, northern Ladakh: linking Kohistan to Tibet. In *Tectonics of Nanga Parbat Syntaxis and the Western Himalaya* (ed. M Asif Khan), pp. 253–75. *Geological Society of London, Special Publication* no. **170**.

White LT, Ahmed T, Ireland TR, Lister GS and Forster MA (2011) Deconvolving episodic age spectra from zircons of the Ladakh Batholith, northwest Indian Himalaya. *Chemical Geology* **289**, 179–96.

White AJR and Chappell BW (1977) Ultrametamorphism and granitoid genesis. *Tectonophysics* **43**, 7–22.

Winchester JA and Floyd PA (1977) Geochemical discrimination of different magma series and their differentiation products using immobile elements. *Chemical Geology* **20**, 325–43.

Wyatt CL, Privalsky V and Datlu RT (1998) *Recommended Practice: Symbols, Units and Uncertainty Analysis for Radiometric Sensor Calibration*. Gaithersburg, Maryland: National Institute of Standards and Technology Handbook 152, 128 pp.

Yogibekov D, Sang M, Xiao W, Windley B, Mamadjanov Y, Yang H, Huang P, Aminov J and Vatanbekov F (2020) Late Palaeozoic to Late Triassic northward accretion and incorporation of seamounts along the northern South Pamir: insights from the anatomy of the Pshart accretionary complex. *Geological Journal* **55**, 7837–57. doi: 10.1002/gj.3906.

Zhang J, Shan X and Huang X (2011) Seismotectonics in the Pamir: an oblique transpressional shear and south-directed deep-subduction model. *Geoscience Frontiers* **2**, 1–15. doi: 10.1016/j.gsf.2010.11.002.

Zhu D-C, Zhao Z-D, Niu Y, Dilek Y, Hou Z-Q and Mo X-X (2013) The origin and pre-Cenozoic evolution of the Tibetan Plateau. *Gondwana Research* **23**, 1429–54. doi: 10.1016/j.gr.2012.02.002.